function in an androgen-independent mechanism. It is known that a number of coactivators function as general coactivators for transcription mediated by nuclear receptors. For example RBM14 is known to activate glucocorticoid receptor-, estrogen receptor-, and thyroid hormone receptor-mediated transcription [59]. It has been reported that SFPQ regulates progesterone receptor, thyroid hormone receptor and retinoic acid receptor, suggesting that SFPQ is a general coregulator of nuclear receptors [24, 25]. In germ cells, several specific nuclear receptors are expressed [60, 61]. PSPC1 and SFPQ may regulate transcription mediated by another nuclear receptor in germ cells. Sertoli cells regulate highly organized and precisely synchronized germ cell development by nourishing the germ cells via their secretion products. Activity of AR-mediated transcription in Sertoli cells is regulated by multiple coregulators. Our present study suggests that the DBHS-containing proteins are coactivators of AR transactivation in Sertoli cells and may be determinants of androgen activity during spermatogenesis. In conclusion, PSPC1, NONO, and SFPQ may support spermatogenesis by regulating androgen receptor-mediated transcription in Sertoli cells.

ACKNOWLEDGMENTS

We thank Dr. Naohito Nozaki for antibody production, and M.S. Atsushi Kawaguchi for his helpful discussion.

REFERENCES

1. Russell LD, Ettlin RA, Sinha Hikim AP, Clegg ED. Histological and Histopathological Evaluation of the Testis. Clearwater, FL: Cache River Press; 1990:1–40.
2. Maclean JA 2nd, Wilkinson MF. Gene regulation in spermatogenesis. Curr Top Dev Biol 2005; 71:131–197.
3. Tanaka H, Baba T. Gene expression in spermiogenesis. Cell Mol Life Sci 2005; 62:344–354.
4. Monaco L, Kotaja N, Fienga G, Hogeveen K, Kolthur US, Kimmins S, Brancorsini S, Macho B, Sassone-Corsi P. Specialized rules of gene transcription in male germ cells: the CREM paradigm. Int J Androl 2004; 27:322–327.
5. Kimmins S, Kotaja N, Davidson I, Sassone-Corsi P. Testis-specific transcription mechanisms promoting male germ-cell differentiation. Reproduction 2004; 128:5–12.
6. Kashiwabara S, Noguchi J, Zhuang T, Ohmura K, Honda A, Sugiura S, Miyamoto K, Takahashi S, Inoue K, Ogura A, Baba T. Regulation of spermatogenesis by testis-specific, cytoplasmic poly(A) polymerase TPAP. Science 2002; 298:1999–2002.
7. Mruk DD, Cheng CY. Sertoli-Sertoli and Sertoli-germ cell interactions and their significance in germ cell movement in the seminiferous epithelium during spermatogenesis. Endocr Rev 2004; 25:747–806.
8. Griswold MD. The central role of Sertoli cells in spermatogenesis. Semin Cell Dev Biol 1998; 9:411–416.
9. Syed V, Hecht NB. Disruption of germ cell-Sertoli cell interactions leads to spermatogenic defects. Mol Cell Endocrinol 2002; 186:155–157.
10. Dohle GR, Smit M, Weber RF. Androgens and male fertility. World J Urol 2003; 21:341–345.
11. Chang C, Chen YT, Yeh SD, Xu Q, Wang RS, Guillou F, Lardy H, Yeh S. Infertility with defective spermatogenesis and hypotestosteronemia in male mice lacking the androgen receptor in Sertoli cells. Proc Natl Acad Sci U S A 2004; 101:6876–6881.
12. De Gendt K, Swinnen JV, Saunders PT, Schoonjans L, Dewerchin M, Devos A, Tan K, Atanassova N, Claessens F, Lecureuil C, Heyns W, Carmeliet P, Guillou F, Sharpe RM, Verhoeven G. A Sertoli cell-selective knockout of the androgen receptor causes spermatogenic arrest in meiosis. Proc Natl Acad Sci U S A 2004; 101:1327–1332.
13. Kato S, Matsumoto T, Kawano H, Sato T, Takeyama K. Function of androgen receptor in gene regulations. J Steroid Biochem Mol Biol 2004; 89–90:627–633.
14. Yong EL, Loy CJ, Sim KS. Androgen receptor gene and male infertility. Hum Reprod Update 2003; 9:1–7.
15. Kato S, Sato T, Watanabe T, Takemasa S, Masuhiro Y, Ohtake F, Matsumoto T. Function of nuclear sex hormone receptors in gene regulation. Cancer Chemother Pharmacol 2005; 56:4–9.
16. MacLean HE, Warne GL, Zajac JD. Localization of functional domains in the androgen receptor. J Steroid Biochem Mol Biol 1997; 62:233–242.
17. Heinlein CA, Chang C. Androgen receptor (AR) coregulators: an overview. Endocr Rev 2002; 23(2):175–200.
18. Wang L, Hsu CL, Chang C. Androgen receptor corepressors: an overview. Prostate 2005; 63:117–130.
19. McEwan IJ. Molecular mechanisms of androgen receptor-mediated gene regulation: structure-function analysis of the AF-1 domain. Endocr Relat Cancer 2004; 11:281–293.
20. Ishitani K, Yoshida T, Kitagawa H, Ohta H, Nozawa S, Kato S. p54nrb acts as a transcriptional coactivator for activation function 1 of the human androgen receptor. Biochem Biophys Res Commun 2003; 306:660–665.
21. Ishiguro H, Uemura H, Fujinami K, Ikeda N, Ohta S, Kubota Y. 55 kDa nuclear matrix protein (nmt55) mRNA is expressed in human prostate cancer tissue and is associated with the androgen receptor. Int J Cancer 2003; 105:26–32.
22. Fox AH, Lam YW, Leung AK, Lyon CE, Andersen J, Mann M, Lamond AI. Paraspeckles: a novel nuclear domain. Curr Biol 2002; 12:13–25.
23. Shav-Tal Y, Zipori D. PSF and p54(nrb)/NonO–multi-functional nuclear proteins. FEBS Lett 2002; 531:109–114.
24. Dong X, Shylnova O, Challis JR, Lye SJ. Identification and characterization of the protein-associated splicing factor as a negative co-regulator of the progesterone receptor. J Biol Chem 2005; 280:13329–13340.
25. Mathur M, Tucker PW, Samuels HH. PSF is a novel corepressor that mediates its effect through Sin3A and the DNA binding domain of nuclear hormone receptors. Mol Cell Biol 2001; 21:2298–2311.
26. Gozani O, Patton JG, Reed R. A novel set of spliceosome-associated proteins and the essential splicing factor PSF bind stably to pre-mRNA prior to catalytic step II of the splicing reaction. EMBO J 1994; 13:3356–3367.
27. Rosonina E, Ip JY, Calarco JA, Bakowski MA, Emili A, McCracken S, Tucker P, Ingles CJ, Blencowe BJ. Role for PSF in mediating transcriptional activator-dependent stimulation of pre-mRNA processing in vivo. Mol Cell Biol 2005; 25:6734–6746.
28. Liang S, Lutz CS. p54nrb is a component of the snRNP-free U1A (SF-A) complex that promotes pre-mRNA cleavage during polyadenylation. RNA 2006; 12:111–121.
29. Zhang Z, Carmichael GG. The fate of dsRNA in the nucleus: a p54(nrb)-containing complex mediates the nuclear retention of promiscuously A-to-I edited RNAs. Cell 2001; 106:465–75.
30. Kanai Y, Dohmae N, Hirokawa N. Kinesin transports RNA: isolation and characterization of an RNA-transporting granule. Neuron 2004; 43:513–525.
31. Straub T, Grue P, Uhse A, Lisby M, Knudsen BR, Tange TO, Westergaard O, Boege F. The RNA-splicing factor PSF/p54 controls DNA-topoisomerase I activity by a direct interaction. J Biol Chem 1998; 273:26261–26264.
32. Bladen CL, Udayakumar D, Takeda Y, Dynan WS. Identification of the polypyrimidine tract binding protein-associated splicing factor p54(nrb) complex as a candidate DNA double-strand break rejoining factor. J Biol Chem 2005; 280:5205–5210.
33. Powers CA, Mathur M, Raaka BM, Ron D, Samuels HH. TLS (translocated-in-liposarcoma) is a high-affinity interactor for steroid, thyroid hormone, and retinoid receptors. Mol Endocrinol 1998; 12:4–18.
34. Iacobazzi V, Infantino V, Costanzo P, Izzo P, Palmieri F. Functional analysis of the promoter of the mitochondrial phosphate carrier human gene: identification of activator and repressor elements and their transcription factors. Biochem J 2005; 391:613–621.
35. Deloulme JC, Prichard L, Delattre O, Storm DR. The prooncoprotein EWS binds calmodulin and is phosphorylated by protein kinase C through an IQ domain. J Biol Chem 1997; 272:27369–27377.
36. Adegbola O, Pasternack GR. A pp32-retinoblastoma protein complex modulates androgen receptor-mediated transcription and associates with components of the splicing machinery. Biochem Biophys Res Commun 2005; 334:702–708.
37. Zhang WW, Zhang LX, Busch RK, Farres J, Busch H. Purification and characterization of a DNA-binding heterodimer of 52 and 100 kDa from HeLa cells. Biochem J 1993; 290:267–272.
38. Zolotukhin AS, Michalowski D, Bear J, Smulevitch SV, Traish AM, Peng R, Patton J, Shatsky IN, Felber BK. PSF acts through the human immunodeficiency virus type 1 mRNA instability elements to regulate virus expression. Mol Cell Biol 2003; 23:6618–6630.
39. Xu J, Zhong N, Wang H, Elias JE, Kim CY, Woldman I, Pifl C, Gygi SP, Geula C, Yankner BA. The Parkinson's disease-associated DJ-1 protein is a transcriptional co-activator that protects against neuronal apoptosis. Hum Mol Genet 2005; 14:1231–1241.
40. Emili A, Shales M, McCracken S, Xie W, Tucker PW, Kobayashi R,

Blencowe BJ, Ingles CJ. Splicing and transcription-associated proteins PSF and p54nrb/nonO bind to the RNA polymerase II CTD. RNA 2002; 8:1102–1111.
41. Myojin R, Kuwahara S, Yasaki T, Matsunaga T, Sakurai T, Kimura M, Uesugi S, Kurihara Y. Expression and functional significance of mouse paraspeckle protein 1 on spermatogenesis. Biol Reprod 2004; 71:926–932.
42. Fox AH, Bond CS, Lamond AI. P54nrb Forms a Heterodimer with PSP1 That Localizes to Paraspeckles in an RNA-dependent Manner. Mol Biol Cell 2005; 16:5304–5315.
43. Suzuki T, Kitamura S, Khota R, Sugihara K, Fujimoto N, Ohta S. Estrogenic and antiandrogenic activities of 17 benzophenone derivatives used as UV stabilizers and sunscreens. Toxicol Appl Pharmacol 2005; 203:9–17.
44. Novy M, Pohn R, Andorfer P, Novy-Weiland T, Galos B, Schwarzmayr L, Rotheneder H. EAPP, a novel E2F binding protein that modulates E2F-dependent transcription. Mol Biol Cell 2005; 16:2181–2190.
45. Takahashi S, Inatome R, Yamamura H, Yanagi S. Isolation and expression of a novel mitochondrial septin that interacts with CRMP/CRAM in the developing neurones. Genes Cells 2003; 8:81–93.
46. Tabuchi Y, Ohta S, Yanai N, Obinata M, Kondo T, Fuse H, Asano S. Development of the conditionally immortalized testicular Sertoli cell line TTE3 expressing Sertoli cell specific genes from mice transgenic for temperature sensitive simian virus 40 large T antigen gene. J Urol 2002; 167:1538–1545.
47. Dai T, Vera Y, Salido EC, Yen PH. Characterization of the mouse Dazap1 gene encoding an RNA-binding protein that interacts with infertility factors DAZ and DAZL. BMC Genomics 2001; 2:6.
48. Kurihara Y, Watanabe H, Kawaguchi A, Hori T, Mishiro K, Ono M, Sawada H, Uesugi S. Dynamic changes in intranuclear and subcellular localizations of mouse Prrp/DAZAP1 during spermatogenesis: the necessity of the C-terminal proline-rich region for nuclear import and localization. Arch Histol Cytol 2004; 67:325–333.
49. Sharpe RM, McKinnell C, Kivlin C, Fisher JS. Proliferation and functional maturation of Sertoli cells, and their relevance to disorders of testis function in adulthood. Reproduction 2003; 125:769–784.
50. Meissner M, Dechat T, Gerner C, Grimm R, Foisner R, Sauermann G. Differential nuclear localization and nuclear matrix association of the splicing factors PSF and PTB. J Cell Biochem 2000; 76:559–566.
51. Shav-Tal Y, Lee B, Bar-Haim S, Vandekerckhove J, Zipori D. Enhanced proteolysis of pre-mRNA splicing factors in myeloid cells. Exp Hematol 2000; 28:1029–1038.
52. Traish AM, Huang YH, Ashba J, Pronovost M, Pavao M, McAneny DB, Moreland RB. Loss of expression of a 55 kDa nuclear protein (nmt55) in estrogen receptor-negative human breast cancer. Diagn Mol Pathol 1997; 6:209–221.
53. Boonyaratanakornkit V, Melvin V, Prendergast P, Altmann M, Ronfani L, Bianchi ME, Taraseviciene L, Nordeen SK, Allegretto EA, Edwards DP. High-mobility group chromatin proteins 1 and 2 functionally interact with steroid hormone receptors to enhance their DNA binding in vitro and transcriptional activity in mammalian cells. Mol Cell Biol 1998; 18:4471–4487.
54. Jeong BC, Hong CY, Chattopadhyay S, Park JH, Gong EY, Kim HJ, Chun SY, Lee K. Androgen receptor corepressor-19 kDa (ARR19), a leucine-rich protein that represses the transcriptional activity of androgen receptor through recruitment of histone deacetylase. Mol Endocrinol 2004; 18:13–25.
55. Ozanne DM, Brady ME, Cook S, Gaughan L, Neal DE, Robson CN. Androgen receptor nuclear translocation is facilitated by the f-actin cross-linking protein filamin. Mol Endocrinol 2000; 14:1618–1626.
56. Schrantz N, da Silva Correia J, Fowler B, Ge Q, Sun Z, Bokoch GM. Mechanism of p21-activated kinase 6-mediated inhibition of androgen receptor signaling. J Biol Chem 2004; 279:1922–1931.
57. Yang YS, Yang MC, Tucker PW, Capra JD. NonO enhances the association of many DNA-binding proteins to their targets. Nucleic Acids Res 1997; 25:2284–2292.
58. Kiesler E, Miralles F, Ostlund Farrants AK, Visa N. The Hrp65 self-interaction is mediated by an evolutionarily conserved domain and is required for nuclear import of Hrp65 isoforms that lack a nuclear localization signal. J Cell Sci 2003; 116:3949–3956.
59. Iwasaki T, Chin WW, Ko L. Identification and characterization of RRM-containing coactivator activator (CoAA) as TRBP-interacting protein, and its splice variant as a coactivator modulator (CoAM). J Biol Chem 2001; 276:33375–33383.
60. Hummelke GC, Cooney AJ. Reciprocal regulation of the mouse protamine genes by the orphan nuclear receptor germ cell nuclear factor and CREMtau. Mol Reprod Dev 2004; 68:394–407.
61. Lee CH, Chinpaisal C, Wei LN. A novel nuclear receptor heterodimerization pathway mediated by orphan receptors TR2 and TR4. J Biol Chem 1998; 273:25209–25215.

Neuroscience 155 (2008) 780–788

IDENTIFICATION OF GENES THAT RESTRICT ASTROCYTE DIFFERENTIATION OF MIDGESTATIONAL NEURAL PRECURSOR CELLS

T. SANOSAKA,[a] M. NAMIHIRA,[a] H. ASANO,[a] J. KOHYAMA,[a] K. AISAKI,[b] K. IGARASHI,[b] J. KANNO[b] AND K. NAKASHIMA[a]*

[a]*Laboratory of Molecular Neuroscience, Graduate School of Biological Sciences, Nara Institute of Science and Technology, 8916-5, Takayama, Ikoma, Nara 630-0101, Japan*

[b]*Division of Cellular and Molecular Toxicology, Biological Safety Research Center, National Institutes of Health Sciences, 1-18-1, Kamiyoga, Setagaya-ku, Tokyo 158-8501, Japan*

Abstract—During development of the mammalian CNS, neurons and glial cells (astrocytes and oligodendrocytes) are generated from common neural precursor cells (NPCs). However, neurogenesis precedes gliogenesis, which normally commences at later stages of fetal telencephalic development. Astrocyte differentiation of mouse NPCs at embryonic day (E) 14.5 (relatively late gestation) is induced by activation of the transcription factor signal transducer and activator of transcription (STAT) 3, whereas at E11.5 (mid-gestation) NPCs do not differentiate into astrocytes even when stimulated by STAT3-activating cytokines such as leukemia inhibitory factor (LIF). This can be explained in part by the fact that astrocyte-specific gene promoters are highly methylated in NPCs at E11.5, but other mechanisms are also likely to play a role. We therefore sought to identify genes involved in the inhibition of astrocyte differentiation of NPCs at midgestation. We first examined gene expression profiles in E11.5 and E14.5 NPCs, using Affymetrix GeneChip analysis, applying the Percellome method to normalize gene expression level. We then conducted *in situ* hybridization analysis for selected genes found to be highly expressed in NPCs at midgestation. Among these genes, we found that *N-myc* and high mobility group AT-hook 2 (*Hmga2*) were highly expressed in the E11.5 but not the E14.5 ventricular zone of mouse brain, where NPCs reside. Transduction of *N-myc* and *Hmga2* by retroviruses into E14.5 NPCs, which normally differentiate into astrocytes in response to LIF, resulted in suppression of astrocyte differentiation. However, sustained expression of *N-myc* and *Hmga2* in E11.5 NPCs failed to maintain the hypermethylated status of an astrocyte-specific gene promoter. Taken together, our data suggest that astrocyte differentiation of NPCs is regulated not only by DNA methylation but also by genes whose expression is controlled spatio-temporally during brain development.

*Corresponding author. Tel: +81-743-72-5471; fax: +81-743-72-5479.
E-mail address: kin@bs.naist.jp (K. Nakashima).

Abbreviations: bHLH, basic helix–loop–helix; BMP, bone morphogenetic protein; CNTF, ciliary neurotrophic factor; CT-1, cardiotrophin-1; DIG, digoxigenin; E, embryonic day; Gapdh, glyceraldehyde-3-phosphate dehydrogenase; GEO, Gene Expression Omnibus; *gfap*, glial fibrillary acidic protein; *Hmga2*, high mobility group AT-hook 2; JAK, janus kinase; LIF, leukemia inhibitory factor; NPC, neural precursor cell; SSC, sodium chloride sodium citrate; STAT, signal transducer and activator of transcription.

Key words: *N-myc*, *Hmga2*, epigenetics, Percellome method, differentiation.

The mammalian CNS is composed of neurons, astrocytes, and oligodendrocytes. Although these three cell types are derived from common multipotent neural precursor cells (NPCs), their differentiation is spatially and temporally regulated during development (Temple, 2001). Fetal telencephalic NPCs divide symmetrically in early gestation to increase their own numbers, and then undergo neurogenesis through mostly asymmetric divisions. Toward the end of the neurogenic phase, NPCs acquire multipotentiality to generate astrocytes and oligodendrocytes as well as neurons. It has recently become apparent that NPC fate determination is controlled by both extracellular cues, including cytokine signaling, and intracellular programs such as epigenetic gene regulation (Edlund and Jessell, 1999; Takizawa et al., 2001; Hsieh and Gage, 2004).

Interleukin (IL) -6 family cytokines such as cardiotrophin-1 (CT-1), leukemia inhibitory factor (LIF) and ciliary neurotrophic factor (CNTF) activate the janus kinase (JAK) –signal transducer and activator of transcription (STAT) signaling pathway and are known to induce astrocyte differentiation of NPCs (Bonni et al., 1997; Rajan and McKay, 1998). Gene knockouts of LIF (Bugga et al., 1998), LIF receptor β (Koblar et al., 1998), the common receptor component gp130 (Nakashima et al., 1999a) and STAT3 (He et al., 2005) all result in impaired astrocyte differentiation *in vivo*, emphasizing the contribution of JAK-STAT signaling to astrogliogenesis in the developing CNS. Bone morphogenetic proteins (BMPs) are another group of astrocyte-inducing cytokines. They synergistically induce astrocytic differentiation of NPCs via formation of a complex between STATs and BMP-activated transcription factor Smads, bridged by the transcriptional coactivators p300/CBP (Nakashima et al., 1999b).

In addition to these extracellular factors, intracellular programs and factors also play critical roles to regulate astrocytic differentiation of NPCs. We have previously shown that a CpG dinucleotide within a STAT3-binding element (TTC*CG*AGAA) in the astrocytic marker glial fibrillary acidic protein (*gfap*) gene promoter is highly methylated in NPCs at midgestation (embryonic day (E)11.5), when the cells differentiate only into neurons but not into astrocytes. Since STAT3 does not bind to the methylated cognate sequence, NPCs at midgestation do not express *gfap* even when stimulated by STAT3-activating cytokines such as LIF. As gestation proceeds, the STAT3-binding

0306-4522/08$32.00+0.00
doi:10.1016/j.neuroscience.2008.06.039

site becomes gradually demethylated in NPCs, enabling them to express *gfap* in response to LIF stimulation (Takizawa et al., 2001). Thus, we have proposed that DNA methylation is a critical cell-intrinsic determinant of astrocyte differentiation during brain development. However, the important question of how this astrocyte-specific gene promoter becomes demethylated in NPCs remains unanswered.

Neurogenic basic helix–loop–helix (bHLH) transcription factors have been also shown to regulate astrocyte differentiation during early neural development. Mice carrying mutations in *mash1* and *math3* (Tomita et al., 2000), or, to a lesser extent, *mash1* and *ngn2* (Nieto et al., 2001) exhibit decreased neurogenesis and premature astrogliogenesis. Conversely, overexpression of neurogenic bHLH factors, either *in vivo* during the gliogenic period (Cai et al., 2000) or in cultured NPCs exposed to CNTF (Sun et al., 2001), promotes neurogenesis at the expense of astrogliogenesis. A possible mechanism underlying the repressive effect on astrogliogenesis is that Ngn1 binds to p300/CBP and sequesters them away from STAT3, thereby preventing STAT3 from activating astrocytic gene expression (Sun et al., 2001). Such a mechanism may ensure the restriction of astrocyte differentiation in NPCs that would otherwise differentiate into neurons under the influence of high-level neurogenic bHLH factor expression during the neurogenic period.

Although these studies have provided us with an integrated insight into the mechanism of neurogenic-to-gliogenic switching in NPCs, they do not preclude the involvement of other, as yet unknown, factors. To identify such factors, we first in this study examined gene expression profiles of mid- and late-gestational NPCs by Affymetrix GeneChip analysis, which is widely used to obtain a complete picture of developmental stage-specific gene expression (Abramova et al., 2005; Ajioka et al., 2006). We then performed *in situ* hybridization experiments to investigate the spatio-temporal expression pattern of genes that were found to be highly expressed in midgestational NPCs. Two genes, *N-myc* and high mobility group AT-hook 2 (*Hmga2*), were highly expressed in the ventricular zone of E11.5 but not of E14.5 mouse brain. Transduction of *N-myc* and *Hmga2* into E14.5 NPCs resulted in suppression of astrocyte differentiation, even in the presence of LIF. However, the prolonged expression of these genes in E11.5 NPCs failed to preserve the hypermethylated status of the astrocyte-specific *gfap* promoter. These results suggest that the inhibition of astrocyte differentiation in midgestational NPCs is regulated not only by DNA methylation of astrocyte-specific gene promoters but also by transcription-regulating factors whose expression is controlled spatiotemporally during brain development.

EXPERIMENTAL PROCEDURES

NPC culture

Timed-pregnant ICR mice were used to prepare NPCs. The protocols described below were carried out according to the animal experimentation guidelines of Nara Institute of Science and Technology that comply with National Institutes of Health Guide for Care and Use of Laboratory Animals. All efforts were made to minimize the number of animals used and their suffering. NPCs were prepared from telencephalons of E11.5 and E14.5 mice and cultured as described previously (Nakashima et al., 1999b). Briefly, the telencephalons were triturated in Hanks' balanced salt solution by mild pipetting with a 1-ml pipet tip (Gilson, Middleton, WI, USA). Dissociated cells were cultured in N2-supplemented Dulbecco's Modified Eagle's Medium with F12 (GIBCO, Grand Island, NY, USA) containing 10 ng/ml basic FGF (R&D Systems, Minneapolis, MN, USA) (N2/DMEM/F12/bFGF) on culture dishes (Nunc, Naperville, IL, USA) or chamber slides (Nunc) which had been precoated with poly-L-ornithine (Sigma, St. Louis, MO, USA) and fibronectin (Sigma).

Immunocytochemistry

E11.5 and E14.5 NPCs cultured on coated chamber slides were washed with PBS, fixed in 4% paraformaldehyde in PBS, and stained with the following primary antibodies: rabbit anti-SOX2 (1:1000, Chemicon, Temecula, CA, USA), mouse anti-βIII-tubulin (1:500, Sigma), rabbit anti-GFAP (1:2000, Dako, High Wycombe, UK). The following secondary antibodies were used: Alexa488-conjugated goat anti-rabbit IgG (1:500, Molecular Probes, Eugene, OR, USA), Cy3-conjugated goat anti-mouse IgG (1:500, Chemicon). Nuclei were stained using bisbenzimide H33258 fluorochrome trihydrochloride (Nacalai Tesque, Kyoto, Japan). All experiments were independently replicated at least three times.

Sample preparation and GeneChip analysis

These procedures were conducted according to the Percellome method (Kanno et al., 2006) to normalize mRNA expression values to sample cell numbers by adding external spike mRNAs to the sample in proportion to the genomic DNA concentration and utilizing the spike RNA quantity data as a dose-response standard curve for each sample. Cells cultured on coated dishes were washed with PBS, lysed in 500 ml of RLT buffer (Qiagen K.K., Tokyo, Japan) and transferred to a 1.5-ml tube. Two separate 10-μl aliquots were treated with DNAse-free RNase A (Nippon Gene, Tokyo, Japan) for 30 min at 37 °C, followed by proteinase K (Roche Diagnostics, Mannheim, Germany) for 3 h at 55 °C, and then transferred to a 96-well black plate. PicoGreen fluorescent dye (Molecular Probes) was added to each well, and then incubated for 2 min at 30 °C. The DNA concentration was measured using a 96-well fluorescence plate reader with excitation at 485 nm and emission at 538 nm. Lamda phage DNA (PicoGreen kit, Molecular Probes) was used as standard. The appropriate amount of spike RNA cocktail was added to the sample homogenates in proportion to their DNA concentration. Five independent *Bacillus subtilis* poly-A RNAs were included in the grade-dosed spike cocktail. Total RNAs were purified using an RNeasy Mini kit (Qiagen), according to the manufacturer's instructions. First-strand cDNAs were synthesized by incubating 5 μg of total RNA with 200 U SuperScript II reverse transcriptase (Invitrogen, Carlsbad, CA, USA) and 100 pmol T7-$(dT)_{24}$ primer [5′-GGCCAGTGAATTGTAATACGACTCACTATAGGGAGGCGG-$(dT)_{24}$-3′]. After second-strand synthesis, the double-stranded cDNAs were purified using a GeneChip Sample Cleanup Module (Affymetrix, Washington, DC, USA), according to the manufacturer's instructions, and labeled by *in vitro* transcription using a BioArray HighYield RNA transcript labeling kit (Enzo Life Sciences, Farmingdale, NY, USA). The labeled cRNA was then purified using a GeneChip Sample Cleanup Module (Affymetrix) and treated with fragmentation buffer at 94 °C for 35 min. For hybridization to a GeneChip Mouse Genome 430 2.0 Array (Affymetrix), 15 μg of fragmented cRNA probe was incubated with 50 pM control oligonucleotide B2, 1× eukaryotic hybridization control (1.5 pM BioB, 5 pM BioC, 25 pM BioD and 100 pM Cre), 0.1 mg/ml herring sperm

DNA, 0.5 mg/ml acetylated BSA and 1× manufacturer-recommended hybridization buffer in a 45 °C rotisserie oven for 16 h. Washing and staining were performed in a GeneChip Fluidics Station (Affymetrix) using the appropriate antibody amplification, washing and staining protocols. The phycoerythrin-stained arrays were scanned as digital image files, which were analyzed with GeneChip Operating Software (Affymetrix). The expression data were converted to copy numbers of mRNA per cell by the Percellome method, quality controlled, and analyzed using Percellome software (Kanno et al., 2006). The GeneChip data have been deposited in the NCBI Gene Expression Omnibus (GEO; http://www.ncbi.nlm.nih.gov/geo/) and is accessible through GEO series accession number GSE 10796.

Quantitative real-time RT-PCR

Quantitative real-time PCR was performed to confirm the results of GeneChip analysis. RNAs from E11.5 and E14.5 NPCs were reverse transcribed using Superscript II (Invitrogen) and amplified by PCR, with a specific pair of primers for each gene, using the Mx3000P system (Stratagene, La Jolla, CA, USA). The expression of target genes was normalized to that of glyceraldehyde-3-phosphate dehydrogenase (*Gapdh*). The gene-specific primers were as follows: mouse N-myc: N-myc-S, 5′-aactatgctgcaccctcacc-3′; N-myc-AS, 5′-tagcaagtccgagcgtgttc-3′; mouse Hmga2: Hmga2-S, 5′-ggcagccgtccacatcag-3′; Hmga2-AS, 5′-taatcctcctctgcggactc-3′; mouse Sox11: Sox11-S, 5′-gagcctgtacgacgaagtgc-3′; Sox11-AS, 5′-tgaacaccaggtcggagaag-3′; mouse Bhlhb5: Bhlhb5-S, 5′-gttgcgcctcaacatcaac-3′; Bhlhb5-AS, 5′-acttttgcagaggctggac-3′; mouse Bcl11a: Bcl11a-S, 5′-gcatcaagctggagaaggag-3′; Bcl11a-AS, 5′-gagcttccatccgaaaactg-3′; mouse Gapdh: Gapdh-S, 5′-accacagtccatgccatcac-3′; Gapdh-AS, 5′-tccaccaccctgttgctgta-3′.

In situ hybridization

Digoxigenin- (DIG; Roche) labeled cRNA probes were synthesized for each gene, following the manufacturer's instructions. Cryosections were washed with PBS and fixed with 4% PFA. After fixation, sections were incubated in prehybridization solution (5× sodium chloride sodium citrate (SSC), 1% SDS, 50 μg/ml yeast transfer RNA, 50 μg/ml heparin in 50% formamide) at 70 °C for 1 h and hybridized with 500 ng/ml of DIG-labeled cRNA probes at 65 °C for 16 h. After three washes with wash solution 1 (5× SSC, 1% SDS in 50% formamide) and wash solution 3 (2× SSC in 50% formamide), sections were blocked with 10% normal sheep serum in TBST at room temperature for 1 h and then incubated with 1:1000 alkaline phosphatase-conjugated anti-DIG antibody (Roche) at 4 °C for 16 h. After four washes with TBST, hybridized probes were visualized with 5-bromo-4-chloro-3 indolylphosphate and nitro blue tetrazolium chloride.

Recombinant retrovirus construction and infection

Human *N-myc* and mouse *Hmga2* cDNAs were cloned into the expression vector pMYs, which contains an internal ribosome entry site followed by the region upstream of the *EGFP* gene (Morita et al., 2000). The Plat-E packaging cell line was transiently transfected with the retrovirus DNA by Trans-IT 293 (Mirus, Madison, WI, USA) (Morita et al., 2000). On the following day, the medium was replaced with N2/DMEM/F12/bFGF, and the cells were cultured in this medium for 1 day before virus was collected.

Fluorescence activated cell sorting

Virus-infected E11.5 NPCs were cultured for 4 days, after which GFP-labeled cells were sorted using a FACS Vantage (Becton Dickinson, Franklin Lakes, NJ, USA) at a flow rate of less than 1500 events/s; gating parameters were set by side and forward scatter to eliminate debris, dead and aggregated cells. After sorting, genomic DNA was extracted and used for bisulfite sequencing.

Bisulfite sequencing

Sodium bisulfite treatment of genomic DNA was performed using a Methylamp DNA Modification kit (Epigentek, Brooklyn, NY, USA), according to the manufacturer's instructions. The region in the *gfap* promoter containing the STAT-binding site of the bisulfite-treated genomic DNA was amplified by PCR using the following primers: GFmS (5′-GGGATTTATTAGGAGAATTTTAGAAGTAG-3′), GFmAS (5′-TCTACCCATACTTAAACTTCTAATATCTAC-3′). The PCR products were cloned into pT7Blue vector (Novagen, Madison, WI, USA) and at least 12 randomly selected clones were sequenced.

RESULTS

Preparation of NPCs from different developmental stages and comparison of their gene expression profiles by GeneChip analysis

E11.5 NPCs do not differentiate into astrocytes, even in the presence of the astrocyte-inducing cytokine LIF, in contrast to 4-day cultured E14.5 NPCs (Takizawa et al., 2001). As a first step toward identifying factors involved in the inhibition of astrocyte differentiation of NPCs at midgestation, we examined the gene expression profiles of E11.5 and E14.5 NPCs.

E11.5 and E14.5 NPCs were isolated from embryonic telencephalon and cultured as indicated in Fig. 1A. To evaluate the purity of NPCs in each cell population, the cells were stained with antibody against SOX2, an NPC marker (Graham et al., 2003). As shown in Fig. 1B and C, the majority of cells in both populations were positive for SOX2, indicating that NPCs were highly enriched. An Affymetrix mouse genome GeneChip array was chosen to compare expression profiles in the two populations, and we adopted the Percellome method to normalize gene expression from different samples (Kanno et al., 2006). The method enabled us to quantify mRNA molecules per cell based on the measurement of cell by adding a grade-dosed spike cocktail to the samples. We excluded genes whose transcript copy number was below six per cell. Scatter plots illustrating the differences between E11.5 and E14.5 NPCs are shown in Fig. 1D; 194 genes were expressed at >fivefold higher level in E11.5 NPCs than in E14.5 NPCs (Fig. 1D, light blue zone). Of these, 102 were known genes, and were classified by functional category (Fig. 1E). Since we wished to identify negative regulators of astrocyte differentiation, or factors involved in the epigenetic modification in midgestational NPCs, we focused on transcription-related genes (Fig. 1E, red). These 21 genes are listed in Table 1, and five (*N-myc*, *Hmga2*, *Bhlhb5*, *Sox11*, *Bcl11a*) were selected for further analysis because they have been reported to play roles in cell growth, differentiation, and chromatin remodeling in other types of stem cells (Sawai et al., 1990; Zhou et al., 1995; Saiki et al., 2000; Knoepfler et al., 2002; Brunelli et al., 2003; Sock et al., 2004).

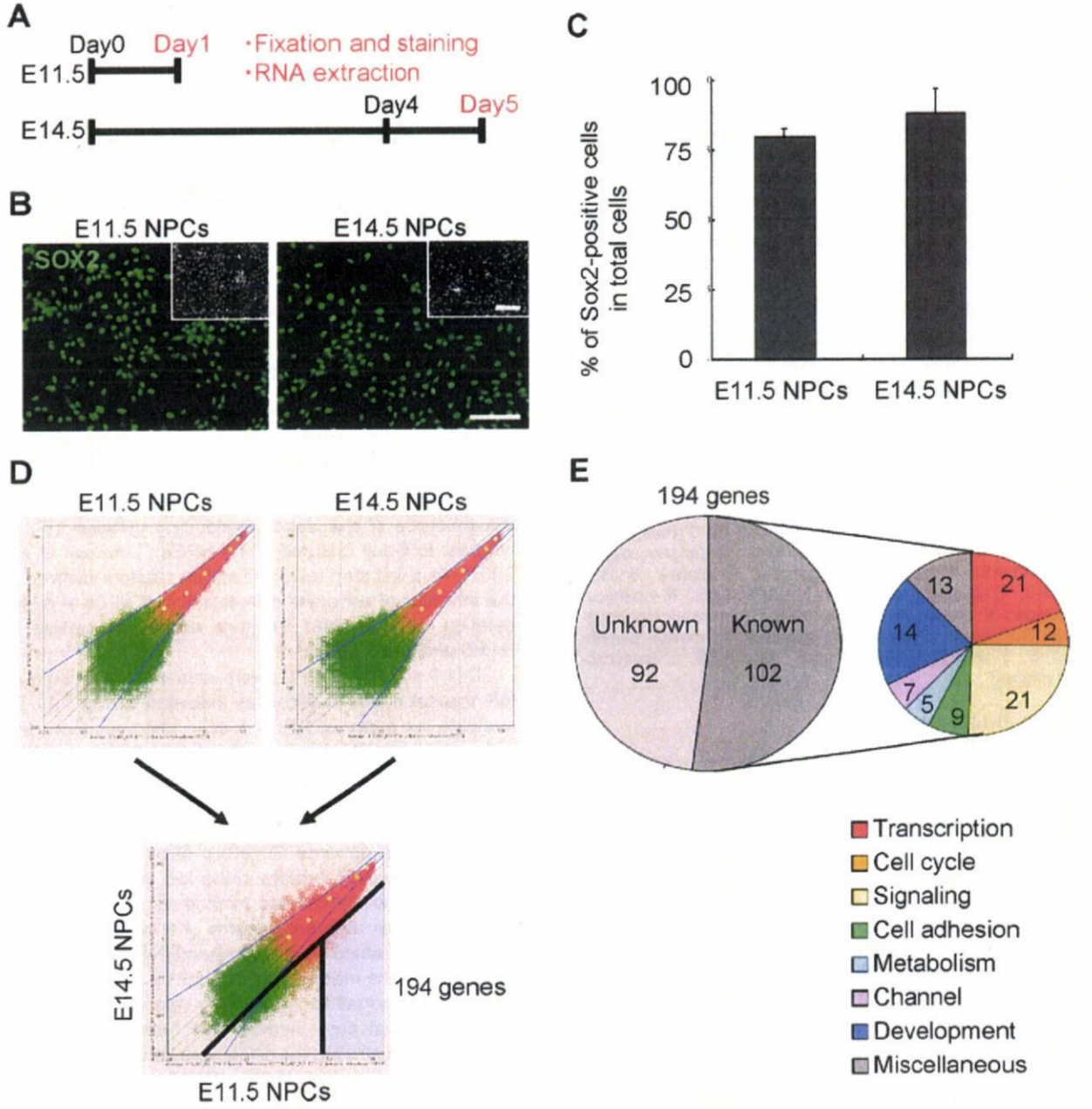

Fig. 1. Comparison of gene expression profiles in E11.5 and E14.5 NPCs. (A) Schematic of experimental protocol. NPCs isolated from E11.5 mouse telencephalon were plated (day 0) and used on the following day for immunostaining and RNA extraction (day 1). NPCs isolated at E14.5 were expanded for 4 days and replated on day 4. On day 5, these cells were fixed for immunostaining. RNA was also extracted. (B) E11.5 and E14.5 NPCs were stained with antibody against Sox2 (green). Scale bar=25 μm. Insets: Hoechst nuclear staining of each field. Scale bar=25 μm. (C) The percentage of Sox2-positive cells in E11.5 and E14.5 NPCs was quantified. Mean±S.D. (D) Scatter plots of E11.5 (upper left) and E14.5 (upper right) samples obtained from GeneChip analysis indicated no significant change between independent experiments with the same sample. Overview (lower plot) of gene expression change was compared between each sample. One hundred ninety-four genes were expressed at >fivefold higher level in E11.5 NPCs than E14.5 NPCs (light blue zone). (E) Of the 194 genes that were highly expressed in E11.5 NPCs, known genes were classified according to Affymetrix gene ontology. For interpretation of the references to color in this figure legend, the reader is referred to the Web version of this article.

Table 1. Transcription-related genes highly expressed in E11.5 NPCs

Probe set ID	GenBank ID	Gene symbol	E11.5 NPCs	E14.5 NPCs	E11.5/ E14.5
1433919_at	AV302111	*Asb4*	9.8	0.5	19.6
1419406_a_at	NM_016707	***Bcl11a***	13.8	1.8	7.7
1418271_at	NM_021560	***Bhlhb5***	10.6	1.2	8.8
1452207_at	Y15163	*Cited2*	16.7	2.6	6.4
1449470_at	NM_010053	*Dlx1*	13.8	2.4	5.8
1448877_at	NM_010054	*Dlx2*	9.8	1.8	5.4
1449863_a_at	NM_010056	*Dlx5*	11.2	0.7	16.0
1459211_at	AW546128	*Gli2*	8.0	1.5	5.3
1456067_at	AW546010	*Gli3*	20.6	2.1	9.8
1422851_at	X58380	***Hmga2***	25.5	0.5	51.0
1450723_at	BQ176915	*Ils1*	8.6	0.1	86.0
1427300_at	D49658	*Lhx8*	10.5	0.1	105.0
1417155_at	BC005453	***N-myc***	8.2	1.2	6.8
1415811_at	BB702754	*NP95*	12.6	2.1	6.0
1421193_a_at	NM_016768	*Pbx3*	12.3	1.6	7.7
1417400_at	NM_030690	*Rai14*	11.0	1.6	6.9
1435856_x_at	AV310148	*Smarcb1*	8.0	1.6	5.0
1431255_at	BB656631	***Sox11***	38.7	6.2	6.2
1450034_at	AW214029	*Stat1*	9.6	1.8	5.3
1416711_at	NM_009322	*Tbr1*	9.8	0.2	49.0
1423424_at	BB732077	*Zic3*	11.2	0.5	22.4

Genes reported to participate in cell growth, differentiation and chromatin remodeling are shown in boldface.

Spatio-temporal expression patterns of genes highly expressed in E11.5 NPCs

To substantiate the GeneChip results, we extracted RNA from E11.5 and E14.5 NPCs and performed real-time RT-PCR using specific primers for each selected gene. Consistent with the GeneChip analysis, all five genes were highly expressed in E11.5 NPCs compared with E14.5 NPCs (Fig. 2A). We next performed *in situ* hybridization for each gene using E11.5, E14.5 and E17.5 mouse brain sections (Fig. 2B). *N-myc* and *Hmga2* mRNAs were specifically detected in the ventricular zone (VZ) of E11.5 brain, implying that N-myc and Hmga2 play some role in NPCs at this stage. By contrast, *Bhlhb5*, *Sox11* and *Bcl11a* expression was stronger in cortical plate, where postmitotic neurons reside, than in the VZ (Fig. 2B). We therefore decided to analyze the function of N-myc and Hmga2 in more detail.

Transduction of *N-myc* and *Hmga2* inhibits astrocyte differentiation of E14.5 NPCs

We next examined whether N-myc and Hmga2 affect astrocyte differentiation of NPCs. We expressed EGFP alone (control), and EGFP together with either N-myc or Hmga2, using retroviral infection in E14.5 NPCs, in which expression of the endogenous genes is very low. Virus-infected E14.5 NPCs were cultured for 4 days in the presence of LIF to induce astrocyte differentiation, and then stained with antibodies against GFP and GFAP. As shown in Fig. 3A and B, NPCs infected with control virus effectively differentiated into GFAP-positive astrocytes in response to LIF stimulation (42±2.6%). In contrast, GFAP-positive astrocyte differentiation was virtually abolished in cells ectopically expressing N-myc (0.5±0.4%) and Hmga2 (3±2.0%) (Fig. 3A, B). Expression of these genes did not significantly affect neuronal differentiation of NPCs, as assessed by monitoring expression of the neuronal marker βIII-tubulin, compared with the control cells (Fig. 3C, D). We further examined whether the observed suppression of astrocyte differentiation of NPCs infected with viruses encoding N-myc or Hmga2 could be attributed to specific cell-growth inhibition or to cell death. To address this issue, we performed immune staining for the cycling cell marker Ki67 and the apoptotic marker cleaved caspase 3. Although proliferation of NPCs ectopically expressing N-myc or Hmga2 appeared to be slightly enhanced, expression of either gene caused negligible cell death. These results suggest that N-myc and Hmga2 inhibit astrocyte differentiation of NPCs by a mechanism distinct from that of the neurogenic bHLH factors, which enhance neuronal differentiation (Sun et al., 2001).

Continuous expression of N-myc and Hmga2 in E11.5 NPCs fails to preserve the hypermethylated status of an astrocyte-specific gene promoter

We have previously shown that the *gfap* promoter is highly methylated in E11.5 NPCs, and becomes demethylated as gestation proceeds (Takizawa et al., 2001). This demethylation enables NPCs at later developmental stages, E14.5 or thereafter, to respond to LIF and differentiate into GFAP-positive astrocytes. As shown in the foregoing data, expression levels of *N-myc* and *Hmga2* thus seemed to be reduced concurrently with the developmental stage-dependent demethylation of an astrocyte-specific gene promoter; furthermore, ectopic expression of these genes in E14.5 NPCs inhibited GFAP-positive astrocyte differentiation. We therefore hypothesized that sustained expression of N-myc and Hmga2 in E11.5 NPCs might maintain the hypermethylated status of the *gfap* promoter. To test this, we infected E11.5 NPCs with viruses expressing EGFP alone and EGFP together with either N-myc or Hmga2 and cultured them for 4 days. GFP-positive cells were sorted by FACS and their genomic DNAs were extracted for bisulfite sequencing. As observed in the previous study (Takizawa et al., 2001), the *gfap* promoter including the STAT3 site became demethylated to about 65% in control virus-infected cells after the 4-day culture, and this was also the case for both N-myc- and Hmga2-expressing virus-infected cells (Fig. 3E, F). These results indicate that sustained expression of N-myc and Hmga2 in E11.5 NPCs does not affect the process of demethylation in this astrocyte-specific gene promoter. On the other hand, when 4-day-cultured control virus-infected E11.5 NPCs were then stimulated with LIF for an additional 4 days, GFAP-positive astrocytes appeared, probably due to demethylation in the promoter, whereas neither *N-myc* nor *Hmga2* virus-infected cells gave rise to astrocytes even in the presence of LIF (data not shown). These results suggest that N-myc and Hmga2 inhibit precocious astrocyte differentiation of midgestational NPCs independent of the DNA methylation status of an astrocyte-specific gene promoter.

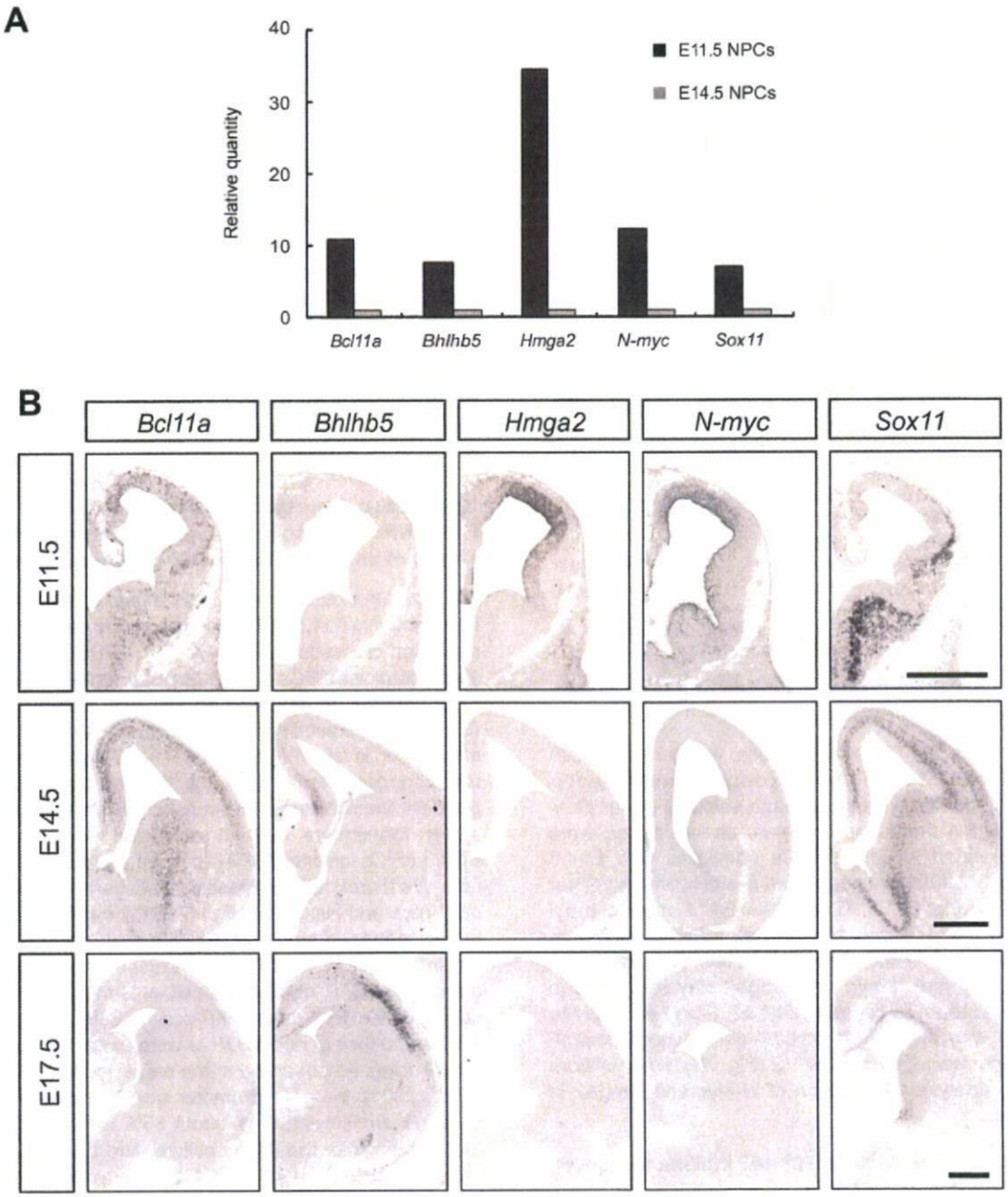

Fig. 2. *N-myc* and *Hmga2* are highly expressed in the VZ of E11.5 mouse brain. (A) Gene-specific real-time RT-PCR was performed to validate GeneChip analysis data. (B) *In situ* hybridization was performed for E11.5, E14.5 and E17.5 mouse brain sections. No signal was detected when sense-probes for each gene were used (data not shown). Scale bar=500 μm.

DISCUSSION

In this study, we compared NPC gene expression profiles at different developmental stages using Affymetrix GeneChips and the Percellome method, and then analyzed by *in situ* hybridization the spatio-temporal expression patterns of genes which were highly expressed in E11.5 NPCs. We found that *N-myc* and *Hmga2* were specifically expressed in E11.5 NPC both *in vivo* and *in vitro* and, furthermore, that the transduction of these genes into NPCs suppressed LIF-induced astrocytic differentiation without affecting DNA demethylation of the astrocyte-specific *gfap* gene promoter.

The basic HLH leucine zipper transcription factor N-myc,a member of the myc family of oncogenes, is a nuclear phosphoprotein exhibiting site-specific DNA-binding activity (Ramsay et al., 1986; Alex et al., 1992), and has

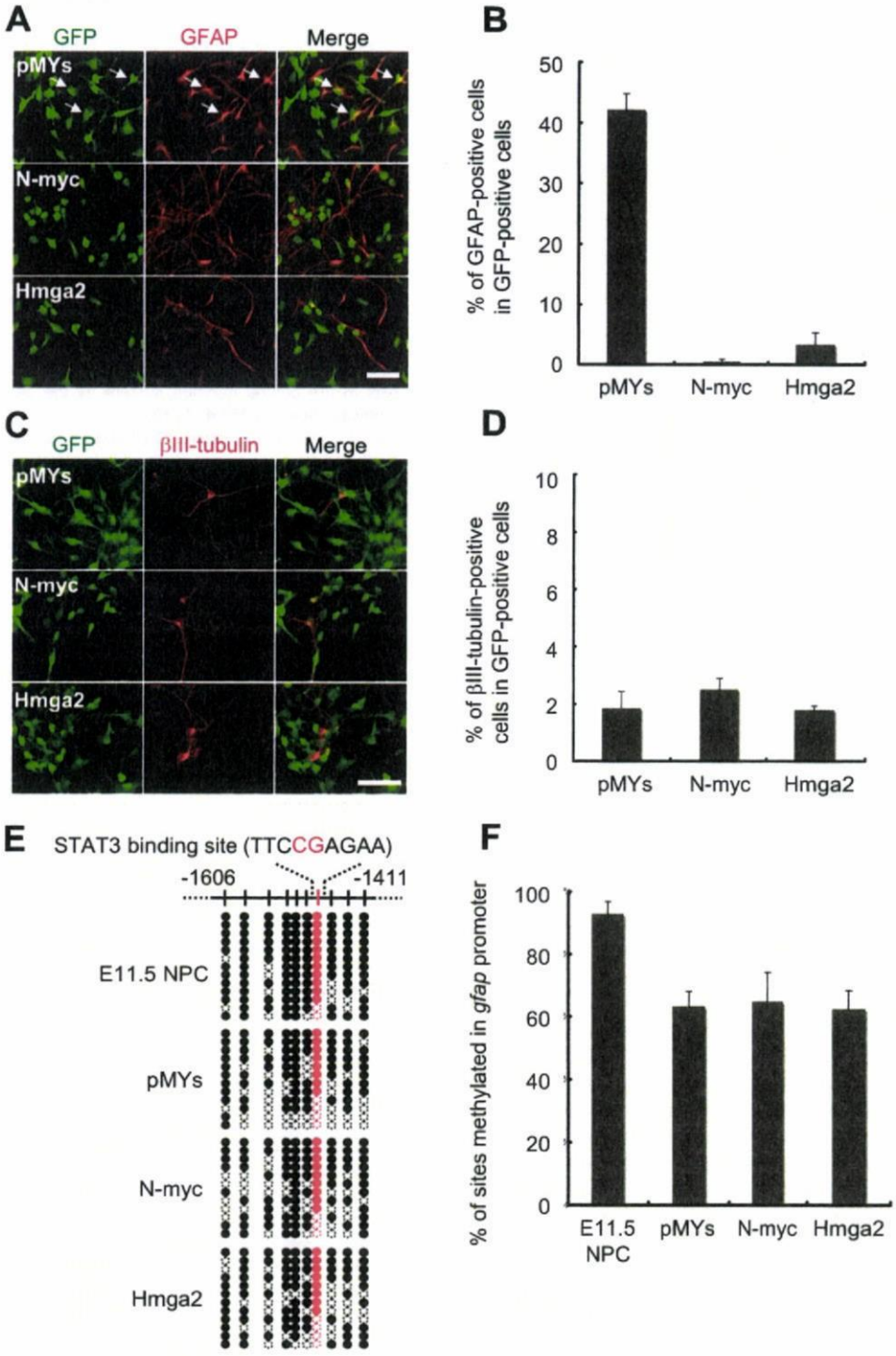

Fig. 3. N-myc and Hmga2 inhibit astrocyte differentiation of NPCs even in the presence of LIF. (A–D) E14.5 NPCs were infected with recombinant retroviruses engineered to express *EGFP* alone (pMYs), and *EGFP* together with either *N-myc* (N-myc) or *Hmga2* (Hmga2), and cultured with LIF (50 ng/ml) for 4 days to induce astrocyte differentiation. The cells were then stained with antibodies against GFP (green) and GFAP (red) (A). Arrows indicate GFP/GFAP double-positive cells. The percentage of GFAP-positive astrocytes in GFP-positive cells was quantified (B). Mean±S.D. The cells were also stained with antibodies against GFP (green) and βIII-tubulin (red) (C). The percentage of βIII-tubulin-positive neurons in GFP-positive cells was quantified (D). Mean±S.D. (E) E11.5 NPCs were infected with recombinant retroviruses engineered to express *EGFP* alone (pMYs), and *EGFP* together with either *N-myc* (N-myc) or *Hmga2* (Hmga2), and subsequently cultured for 4 days. GFP-positive cells were then sorted based on GFP fluorescence, and genomic DNA was extracted for bisulfite sequencing. White and black circles indicate unmethylated and methylated CpG sites, respectively. The E11.5 NPC sample was freshly prepared NPCs from telencephalon at E11.5. The CpG dinucleotide within the STAT3 binding site is indicated in red. (F) Methylation frequency in the *gfap* promoter. Mean±S.D. Scale bars=50 μm (A, C). For interpretation of the references to color in this figure legend, the reader is referred to the Web version of this article.

been reported to be expressed in a wide range of vertebrate tissues, primarily during embryogenesis (Schreiber-Agus et al., 1993). The mice deficient for functional *N-myc* are embryonic lethal (Stanton et al., 1992). Since N-myc has been shown to be a transcriptional activator, it may inhibit astrocyte differentiation via induction of neurogenic bHLH factors such as *Ngn1* (Sun et al., 2001), which have already been suggested to inhibit astrocyte differentiation in midgestational NPCs. However, this scenario seems unlikely because *N-myc* expression in NPCs did not affect neuronal differentiation, as assessed by monitoring expression of the neuronal marker βIII-tubulin (Fig. 3C, D). On the other hand, Hmga2 possesses an acidic C-terminal tail and three individual DNA-binding domains which bind short stretches of AT-rich DNA with high affinity (Reeves, 2001). *Hmga2* is expressed in pluripotent embryonic stem (ES) cells and in most tissues and organs during embryogenesis, but at very low levels or not at all in adult tissues (Zhou et al., 1995). Its function appears to be critical for cell growth, because mice lacking functional *Hmga2* exhibit a pygmy phenotype (Zhou et al., 1995). Recently, it was reported that Hmga2 specifically accumulates on senescent cell chromatin and that it functions as a structural component of senescence-associated heterochromatin foci and as a repressor of proliferation-associated genes (Narita et al., 2006). We therefore expected that Hmga2 would maintain the hypermethylation status of the astrocyte-specific *gfap* promoter via transcription-repressive heterochromatin formation in E11.5 NPCs. However, our results indicate that this is not the case. The mechanism(s) whereby N-myc and Hmga2 inhibit astrocyte differentiation must await further investigation.

Although DNA methylation is a critical cell-intrinsic determinant for the neurogenic-to-astrogliogenic switch and/or astrocyte differentiation of NPCs, many other spatio-temporally expressed extracellular factors such as CT-1, Notch and Wnt1 (Barnabe-Heider et al., 2005; Hirabayashi and Gotoh, 2005; Nagao et al., 2007) and intracellular factors including Ngn (Sun et al., 2001), N-CoR (Hermanson et al., 2002), N-myc and Hmga2 (this study) complement DNA methylation to ensure the sequential differentiation of NPCs during development. Thus, to better understand the mechanism underlying these processes, this study emphasizes the need to take cell-extrinsic cues, cell-intrinsic programs and factors, and their interaction into consideration.

Acknowledgments—We thank Dr. T. Kitamura (Tokyo University) for pMY vector and Plat-E cells. We appreciate Dr. Y. Bessho and T. Matsui for valuable discussions. We also thank Dr. I. Smith for helpful comments and critical reading of the manuscript. We are very grateful to N. Ueda for excellent secretarial assistance. Many thanks to N. Namihira for technical help. We also thank N. Moriyama for technical help with GeneChip analysis. This work has been supported by a Grant-in-Aid for Science Research on Priority Areas and the NAIST Global COE Program (Frontier Biosciences: Strategies for survival and adaptation in a changing global environment) from the Ministry of Education, Culture, Sports, Science and Technology (MEXT) of Japan.

REFERENCES

Abramova N, Charniga C, Goderie SK, Temple S (2005) Stage-specific changes in gene expression in acutely isolated mouse CNS progenitor cells. Dev Biol 283:269–281.

Ajioka I, Maeda T, Nakajima K (2006) Identification of ventricular-side-enriched molecules regulated in a stage-dependent manner during cerebral cortical development. Eur J Neurosci 23:296–308.

Alex R, Sozeri O, Meyer S, Dildrop R (1992) Determination of the DNA sequence recognized by the bHLH-zip domain of the N-Myc protein. Nucleic Acids Res 20:2257–2263.

Barnabe-Heider F, Wasylnka JA, Fernandes KJ, Porsche C, Sendtner M, Kaplan DR, Miller FD (2005) Evidence that embryonic neurons regulate the onset of cortical gliogenesis via cardiotrophin-1. Neuron 48:253–265.

Bonni A, Sun Y, Nadal-Vicens M, Bhatt A, Frank DA, Rozovsky I, Stahl N, Yancopoulos GD, Greenberg ME (1997) Regulation of gliogenesis in the central nervous system by the JAK-STAT signaling pathway. Science 278:477–483.

Brunelli S, Innocenzi A, Cossu G (2003) Bhlhb5 is expressed in the CNS and sensory organs during mouse embryonic development. Gene Expr Patterns 3:755–759.

Bugga L, Gadient RA, Kwan K, Stewart CL, Patterson PH (1998) Analysis of neuronal and glial phenotypes in brains of mice deficient in leukemia inhibitory factor. J Neurobiol 36:509–524.

Cai L, Morrow EM, Cepko CL (2000) Misexpression of basic helix-loop-helix genes in the murine cerebral cortex affects cell fate choices and neuronal survival. Development 127:3021–3030.

Edlund T, Jessell TM (1999) Progression from extrinsic to intrinsic signaling in cell fate specification: a view from the nervous system. Cell 96:211–224.

Graham V, Khudyakov J, Ellis P, Pevny L (2003) SOX2 functions to maintain neural progenitor identity. Neuron 39:749–765.

He F, Ge W, Martinowich K, Becker-Catania S, Coskun V, Zhu W, Wu H, Castro D, Guillemot F, Fan G, de Vellis J, Sun YE (2005) A positive autoregulatory loop of Jak-STAT signaling controls the onset of astrogliogenesis. Nat Neurosci 8:616–625.

Hermanson O, Jepsen K, Rosenfeld MG (2002) N-CoR controls differentiation of neural stem cells into astrocytes. Nature 419: 934–939.

Hirabayashi Y, Gotoh Y (2005) Stage-dependent fate determination of neural precursor cells in mouse forebrain. Neurosci Res 51: 331–336.

Hsieh J, Gage FH (2004) Epigenetic control of neural stem cell fate. Curr Opin Genet Dev 14:461–469.

Kanno J, Aisaki K, Igarashi K, Nakatsu N, Ono A, Kodama Y, Nagao T (2006) "Per cell" normalization method for mRNA measurement by quantitative PCR and microarrays. BMC Genomics 7:64.

Knoepfler PS, Cheng PF, Eisenman RN (2002) N-myc is essential during neurogenesis for the rapid expansion of progenitor cell populations and the inhibition of neuronal differentiation. Genes Dev 16:2699–2712.

Koblar SA, Turnley AM, Classon BJ, Reid KL, Ware CB, Cheema SS, Murphy M, Bartlett PF (1998) Neural precursor differentiation into astrocytes requires signaling through the leukemia inhibitory factor receptor. Proc Natl Acad Sci U S A 95:3178–3181.

Morita S, Kojima T, Kitamura T (2000) Plat-E: an efficient and stable system for transient packaging of retroviruses. Gene Ther 7: 1063–1066.

Nagao M, Sugimori M, Nakafuku M (2007) Cross talk between notch and growth factor/cytokine signaling pathways in neural stem cells. Mol Cell Biol 27:3982–3994.

Nakashima K, Wiese S, Yanagisawa M, Arakawa H, Kimura N, Hisatsune T, Yoshida K, Kishimoto T, Sendtner M, Taga T (1999a) Developmental requirement of gp130 signaling in neuronal survival and astrocyte differentiation. J Neurosci 19:5429–5434.

Nakashima K, Yanagisawa M, Arakawa H, Kimura N, Hisatsune T, Kawabata M, Miyazono K, Taga T (1999b) Synergistic signaling in

fetal brain by STAT3-Smad1 complex bridged by p300. Science 284:479–482.

Narita M, Krizhanovsky V, Nunez S, Chicas A, Hearn SA, Myers MP, Lowe SW (2006) A novel role for high-mobility group a proteins in cellular senescence and heterochromatin formation. Cell 126: 503–514.

Nieto M, Schuurmans C, Britz O, Guillemot F (2001) Neural bHLH genes control the neuronal versus glial fate decision in cortical progenitors. Neuron 29:401–413.

Rajan P, McKay RD (1998) Multiple routes to astrocytic differentiation in the CNS. J Neurosci 18:3620–3629.

Ramsay G, Stanton L, Schwab M, Bishop JM (1986) Human proto-oncogene N-myc encodes nuclear proteins that bind DNA. Mol Cell Biol 6:4450–4457.

Reeves R (2001) Molecular biology of HMGA proteins: hubs of nuclear function. Gene 277:63–81.

Saiki Y, Yamazaki Y, Yoshida M, Katoh O, Nakamura T (2000) Human EVI9, a homologue of the mouse myeloid leukemia gene, is expressed in the hematopoietic progenitors and down-regulated during myeloid differentiation of HL60 cells. Genomics 70:387–391.

Sawai S, Kato K, Wakamatsu Y, Kondoh H (1990) Organization and expression of the chicken N-myc gene. Mol Cell Biol 10:2017–2026.

Schreiber-Agus N, Horner J, Torres R, Chiu FC, DePinho RA (1993) Zebra fish myc family and max genes: differential expression and oncogenic activity throughout vertebrate evolution. Mol Cell Biol 13:2765–2775.

Sock E, Rettig SD, Enderich J, Bosl MR, Tamm ER, Wegner M (2004) Gene targeting reveals a widespread role for the high-mobility-group transcription factor Sox11 in tissue remodeling. Mol Cell Biol 24:6635–6644.

Stanton BR, Perkins AS, Tessarollo L, Sassoon DA, Parada LF (1992) Loss of N-myc function results in embryonic lethality and failure of the epithelial component of the embryo to develop. Genes Dev 6:2235–2247.

Sun Y, Nadal-Vicens M, Misono S, Lin MZ, Zubiaga A, Hua X, Fan G, Greenberg ME (2001) Neurogenin promotes neurogenesis and inhibits glial differentiation by independent mechanisms. Cell 104:365–376.

Takizawa T, Nakashima K, Namihira M, Ochiai W, Uemura A, Yanagisawa M, Fujita N, Nakao M, Taga T (2001) DNA methylation is a critical cell-intrinsic determinant of astrocyte differentiation in the fetal brain. Dev Cell 1:749–758.

Temple S (2001) The development of neural stem cells. Nature 414:112–117.

Tomita K, Moriyoshi K, Nakanishi S, Guillemot F, Kageyama R (2000) Mammalian achaete-scute and atonal homologs regulate neuronal versus glial fate determination in the central nervous system. EMBO J 19:5460–5472.

Zhou X, Benson KF, Ashar HR, Chada K (1995) Mutation responsible for the mouse pygmy phenotype in the developmentally regulated factor HMGI-C. Nature 376:771–774.

(Accepted 13 June 2008)
(Available online 21 June 2008)

Cell

Estrogen Prevents Bone Loss via Estrogen Receptor α and Induction of Fas Ligand in Osteoclasts

Takashi Nakamura,[1,2,9] Yuuki Imai,[1,3,9] Takahiro Matsumoto,[1,2] Shingo Sato,[4] Kazusane Takeuchi,[1] Katsuhide Igarashi,[5] Yoshifumi Harada,[6] Yoshiaki Azuma,[6] Andree Krust,[7] Yoko Yamamoto,[1] Hiroshi Nishina,[4] Shu Takeda,[4] Hiroshi Takayanagi,[4] Daniel Metzger,[7] Jun Kanno,[5] Kunio Takaoka,[3] T. John Martin,[8] Pierre Chambon,[7] and Shigeaki Kato[1,2,*]

[1]Institute of Molecular and Cellular Biosciences, University of Tokyo, Yayoi 1-1-1, Bunkyo-ku, Tokyo 113-0032, Japan

[2]Exploratory Research for Advanced Technology, Japan Science and Technology Agency, Honcho 4-1-8, Kawaguchi, Saitama 332-0012, Japan

[3]Department of Orthopaedic Surgery, Osaka City University Graduate School of Medicine, Asahimachi 1-4-3, Abeno-ku, Osaka, 545-8585, Japan

[4]Tokyo Medical and Dental University, Yushima 1-5-45, Bunkyo-ku, Tokyo 113-8510, Japan

[5]Division of Cellular and Molecular Toxicology, National Institute of Health Sciences, 1-18-1 Kamiyoga, Setagaya-ku, Tokyo 158-8501, Japan

[6]Teijin Institute for Biomedical Research, Asahigaoka 4-3-2, Hino, Tokyo 191-8512, Japan

[7]Institut de Génétique et de Biologie Moleculaire et Cellulaire, Departement of Physiological Genetics / Inserm, U-596 / CNRS, UMR7104 / Université Louis Pasteur, Illkirch, Strasbourg, F-67400 France

[8]St. Vincent's Institute of Medical Research, 9 Princes Street, Fitzroy VIC 3065, Australia

[9]These authors contributed equally to this work.

*Correspondence: uskato@mail.ecc.u-tokyo.ac.jp

DOI 10.1016/j.cell.2007.07.025

SUMMARY

Estrogen prevents osteoporotic bone loss by attenuating bone resorption; however, the molecular basis for this is unknown. Here, we report a critical role for the osteoclastic estrogen receptor α (ERα) in mediating estrogen-dependent bone maintenance in female mice. We selectively ablated ERα in differentiated osteoclasts ($ER\alpha^{\Delta Oc/\Delta Oc}$) and found that $ER\alpha^{\Delta Oc/\Delta Oc}$ females, but not males, exhibited trabecular bone loss, similar to the osteoporotic bone phenotype in postmenopausal women. Further, we show that estrogen induced apoptosis and upregulation of Fas ligand (FasL) expression in osteoclasts of the trabecular bones of WT but not $ER\alpha^{\Delta Oc/\Delta Oc}$ mice. The expression of ERα was also required for the induction of apoptosis by tamoxifen and estrogen in cultured osteoclasts. Our results support a model in which estrogen regulates the life span of mature osteoclasts via the induction of the Fas/FasL system, thereby providing an explanation for the osteoprotective function of estrogen as well as SERMs.

INTRODUCTION

Bone remodeling is a dynamic metabolic process. The destruction or "resorption" of pre-existing bone by mature osteoclasts is followed by the formation of new bone by osteoblasts. Osteoblasts are derived from pleiotropic mesenchymal stem cells in the bone marrow. Mature osteoclasts are multinuclear, macrophage-like cells, derived from hematopoietic stem cells also in the bone marrow. Bone resorption and deposition are tightly coupled, and their balance defines both bone mass as well as quality. The regulation of bone remodeling is complex. A number of systemic hormones and transcription factors directly regulate the proliferation and differentiation of osteoblasts and osteoclasts (Karsenty, 2006; Karsenty and Wagner, 2002; Rodan and Martin, 2000; Teitelbaum and Ross, 2003). Additionally, the indirect cellular communication among groups of bone cells is also physiologically critical for bone growth and remodeling (Martin and Sims, 2005; Mundy and Elefteriou, 2006). The molecular and genetic mechanisms governing bone cell fate have been intensively studied; however, how the life span of bone cells is determined on a molecular level remains elusive.

Estrogen is a key hormone in bone remodeling in several species. The osteoprotective action of estrogen is demonstrable in rodents and is clinically important in humans, particularly older women (Chien and Karsenty, 2005;

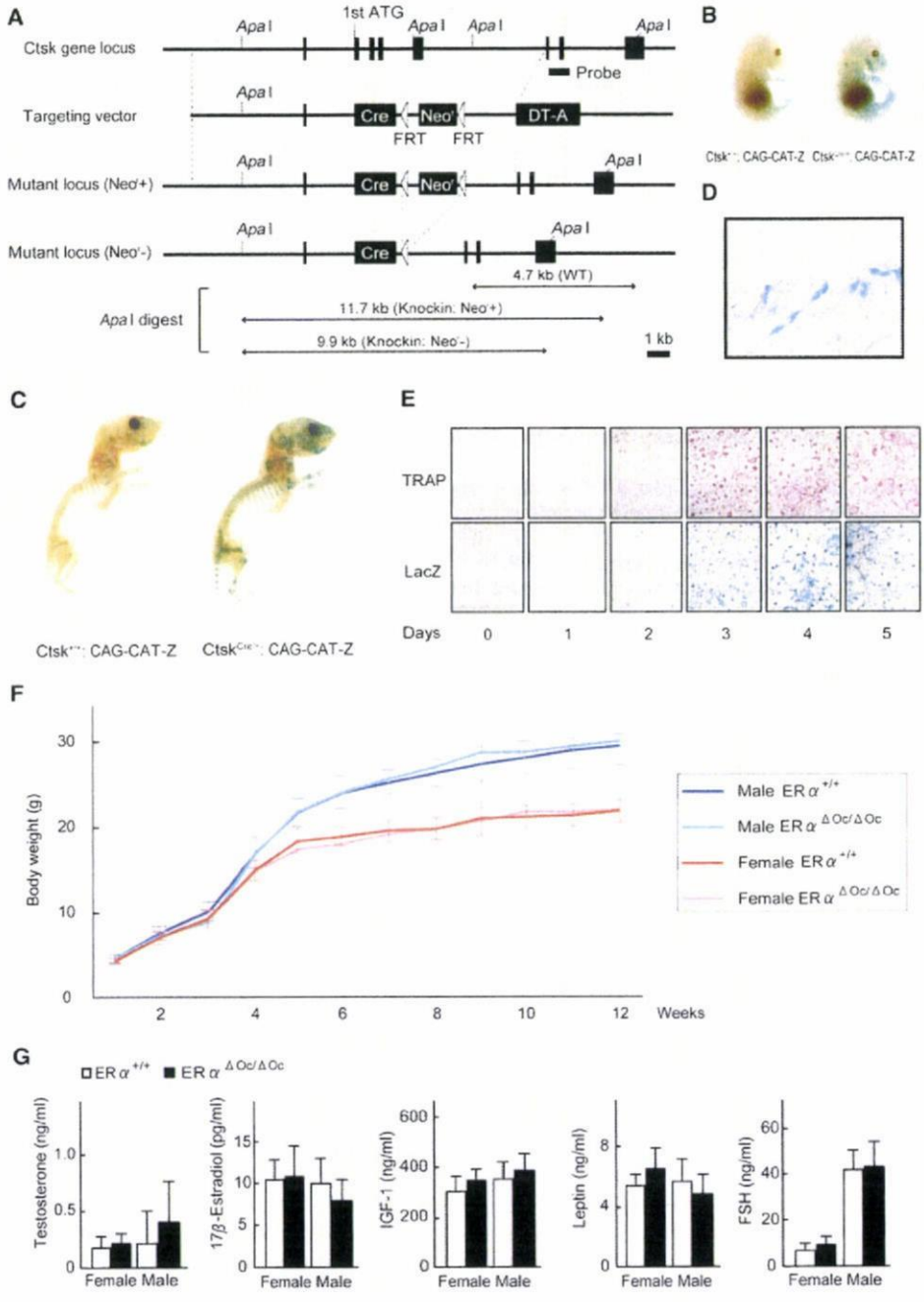

Figure 1. Generation of Knockin Mice Selectively Expressing Cre in Mature Osteoclasts

(A) Illustration of the targeting strategy for insertion of the *Cre* gene into the mouse *Cathepsin K* (*Ctsk*) gene. A targeting vector was generated to contain the *Cre* cDNA at the endogenous ATG start site, followed by a *FRT* (Flp-recombinase target)-flanked *Neo*^{r} cassette. The *DT-A* (diphtheria toxin-A) gene was also inserted to avoid random integrations.

(B and C) *Ctsk-Cre* mice were then crossed with *CAG-CAT-Z* mice. β-galactosidase activity derived from the activated *LacZ* reporter gene was monitored to test if expressed Cre excised the *lox*P sites in mature osteoclasts. LacZ expression patterns reflected the localization patterns of mature osteoclasts in the developing bone at 16.5 days post coitum embryos and in the skeletal tissues of 7-day-old pups.

(D) The LacZ expression induced by Cre-mediated excision was also seen in osteoclasts attached to trabecular bone in the lumber vertebrae of 12-week-old mice.

(E) LacZ expression was induced during osteoclastogenesis. Osteoclast-like cells that differentiated from bone-marrow macrophages following culture in the presence of M-CSF and RANKL were stained with TRAP (tartrate-resistant acid phosphatase), a mature osteoclast marker.

Delmas, 2002; Raisz, 2005; Rodan and Martin, 2000). Estrogen deficiency in postmenopausal women frequently leads to osteoporosis, the most common skeletal disorder. Similarly, ovariectomy clearly produces an osteoporotic bone phenotype in mice. Osteoporotic bone loss is the result of high bone turnover in which bone resorption outpaces bone deposition (Rodan and Martin, 2000; Teitelbaum, 2007). This imbalance in bone turnover that is induced by estrogen deficiency in women and female rodents can be ameliorated with bio-available estrogens including selective estrogen receptor modulators (SERMs) (Riggs and Hartmann, 2003).

Estrogen and SERMs primarily act by regulating gene transcription via estrogen receptors (ERα, ERβ) (Couse and Korach, 1999; Shang and Brown, 2002). ERs belong to the nuclear receptor gene superfamily and act as ligand-inducible transcriptional factors (Mangelsdorf et al., 1995). ER dimers directly or indirectly associate with specific DNA elements in the target gene promoter (Shang and Brown, 2002) and control transcription through reorganizing chromatin structure and histone modifications (Belandia and Parker, 2003). Genetic mouse models (KO mice) lacking ERα ($ER\alpha^{-/-}$) and ERβ ($ER\beta^{-/-}$) provide insights into ER function (Mueller and Korach, 2001; Windahl et al., 2002). In mice, though ERα appears to be the major receptor in most estrogen target tissues including bone (Sims et al., 2003), neither clear bone loss nor high bone turnover is detectable in ERα single or ERα/ERβ double-KO females (Syed and Khosla, 2005; Windahl et al., 2002). This unexpected maintenance of bone mass in female mutants is presumed to be due to unphysiologically elevated levels of other osteoprotective hormones, like androgens. Systemic defects in the hypothalamus caused by ER inactivation appear to impair the negative feedback system of hormone production (Syed and Khosla, 2005). This leads to an excess in estrogen precursors, notably androgens. In fact, the anabolic effects of androgens mediated by the androgen receptor (AR) are evident in female mice (Kawano et al., 2003; Sims et al., 2003). In males, estrogen is also osteoprotective, as is evident by the development of osteopenia in male patients genetically deficient in ERα (Smith et al., 1994) or aromatase activity (Simpson and Davis, 2001). Thus, irrespective of the accumulating clinical and basic research data on the osteoprotective actions of estrogen and SERMs, the molecular basis of this osteoprotection in females remains elusive.

To study the molecular interactions behind the antibone resorptive actions of estrogen in women and female animals, we genetically ablated ERα in mature osteoclasts ($ER\alpha^{\Delta Oc/\Delta Oc}$). Selective ablation of ERα in differentiated osteoclasts ($ER\alpha^{\Delta Oc/\Delta Oc}$) was accomplished by crossing a *Cathepsin K-Cre* knockin mouse with a floxed *ERα* mouse. This resulted in clear trabecular bone loss and high bone turnover associated with increased osteoclast numbers in females but not in males. In the female mutants, further bone loss following ovariectomy was not significant and recovery by estrogen was ineffective in the trabecular areas of long bones and lumbar vertebral bodies. Upregulated expression of *Fas ligand* (*FasL*) gene, and increased apoptosis in differentiated osteoclasts by estrogen was found in the intact bone of wild-type females but undetectable in $ER\alpha^{\Delta Oc/\Delta Oc}$ females. Induction of FasL and apoptosis by estrogen as well as a SERM also required ERα in cultured osteoclasts. Thus, we propose that the osteoprotective actions of estrogen and SERMs are mediated at least in part through osteoclastic ERα in trabecular bone, and the life span of mature osteoclasts is regulated through the activation of the FasL signaling.

RESULTS

Generation of Osteoclast-Specific *ERα* Gene Disruption by Knocked-In *Cre* in the *Cathepsin K* Gene

To specifically disrupt *ERα* gene in mature osteoclasts, we knocked in *Cre* into the gene locus of *Cathepsin K* ($Ctsk^{Cre/+}$) (Figures 1A, S1A, and S1B), a gene known to be expressed in differentiated osteoclastic cells arising from hematopoietic stem cells. This gene is functionally indispensable for mature osteoclasts (Saftig et al., 1998). Only one copy appears enough to support normal bone formation and bone turnover, since heterozygous mutant mice of *Cathepsin K* ($Ctsk^{+/-}$) have no obvious bone phenotype (Gowen et al., 1999; Li et al., 2006; Saftig et al., 1998) . Clear, bone-specific expression of the *Cre* transcript in the adult $Ctsk^{Cre/+}$ mice was observed in the tested tissues (Figure S1C). To confirm Cre protein expression, the $Ctsk^{Cre/+}$ mice were crossed with tester mice (*CAG-CAT-Z*). These mice were genetically engineered to express β-galactosidase by excision of the transcribed stop sequence in front of the *β-galactosidase* gene (*LacZ*) in cells expressing Cre (Sakai and Miyazaki, 1997). β-galactosidase expression visualized by LacZ staining was observed in the bones of 16.5 dpc embryos and 7-day-old pups of $Ctsk^{Cre/+}$; *CAG-CAT-Z* mice. Expression patterns were consistent with the appearance and skeletal localization of functionally mature osteoclasts (Figures 1B and 1C). Histochemical staining of LacZ in the lumbar vertebrae of 12-week-old mice was localized in multinuclear osteoclasts (Figure 1D) but not seen in osteoblasts and osteocytes (Figure S1D) and the hypothalamus (Figure S1E). Since *Cathepsin K* gene expression is evident in differentiated osteoclasts (Saftig et al., 1998), we used an in vitro culture cell system to test whether Cre expression was driven by the endogenous promoter that is induced at the time of osteoclast differentiation. Osteoclast-precursor cells derived from bone marrow

(F) The growth curve of $ER\alpha^{\Delta Oc/\Delta Oc}$ mice was indistinguishable from that of the control mice. Data are represented as mean ± SEM.
(G) Serum hormone levels were normal in 12-week-old $ER\alpha^{\Delta Oc/\Delta Oc}$ (filled column) versus $ER\alpha^{+/+}$ (open column) mice (n = 10–11 animals per genotype). Data are represented as mean ± SEM.

were cytodifferentiated for 1 week in the presence of M-CSF (macrophage colony stimulating factor) and RANKL (receptor activator of NFκB ligand) (Koga et al., 2004). TRAP-positive osteoclasts emerged after 3 days of culture (Figure 1E). The number of TRAP-positive osteoclasts and the number of LacZ-expressing cells simultaneously increased. In the contrast, the LacZ expression was not detected in primary cultured osteoblasts derived from the calvaria (Figure S1F). In view of both our in vivo and in vitro observations, we conclude that the $Ctsk^{Cre/+}$ mouse line expresses Cre in differentiated osteoclasts. Moreover, estrogen response in bone mass control was not distinguishable in between $Ctsk^{Cre/+}$ and $Ctsk^{+/+}$ mice (Figure S2A).

We then crossed floxed $ER\alpha$ mice (Dupont et al., 2000) with $Ctsk^{Cre/+}$ mice to disrupt ERα in differentiated osteoclasts ($ER\alpha^{\Delta Oc/\Delta Oc}$). Excision of the $ER\alpha$ gene (Figure S1G) was confirmed by Southern blotting of DNA from adult female and male (data not shown) bone as well as in cultured mature osteoclasts (Figure S1H). No overt differences were observed in the growth curve, reproduction, or tissues for up to 12 weeks of age (Figure 1F) between the $Ctsk^{Cre/+}$; $ER\alpha^{+/+}$ ($ER\alpha^{+/+}$) and the $Ctsk^{Cre/+}$; $ER\alpha^{flox/flox}$ ($ER\alpha^{\Delta Oc/\Delta Oc}$) mice, with the exception of the female bones. Serum levels of sex hormones and bone remodeling regulators such as IGF-I, leptin, and follicle-stimulating hormone (Sun et al., 2006; Takeda et al., 2002) appeared unchanged in both male and female $ER\alpha^{\Delta Oc/\Delta Oc}$ mice at 12 weeks (Figure 1G).

Osteopenia Occurred in Osteoclast-Specific ERα KO Females But Not Males

The 12-week-old $ER\alpha^{\Delta Oc/\Delta Oc}$ females exhibited a clear reduction in bone mineral density (BMD) in the femurs (Figures 2A–2C) and tibiae (data not shown) when compared with $ER\alpha^{+/+}$ mice. Though cortical bone appeared unaffected, trabecular bone loss (Figure 2A) with significant reduction of trabecular bone volume (BV/TV) (Figure 2F) was clearly seen. This is similar to the osteoporotic abnormalities observed in women during natural menopause or following ovariectomy (Delmas, 2002; Tolar et al., 2004). However, unlike men deficient in aromatase or ERα activity (Simpson and Davis, 2001; Smith et al., 1994), $ER\alpha^{\Delta Oc/\Delta Oc}$ males unexpectedly exhibited no clear bone loss even in the trabecular areas (Figures 2A–2C). In $ER\alpha^{\Delta Oc/\Delta Oc}$ females, both the bone-formation rate, estimated by double-calcein labeling (Figure 2D), as well as the bone-resorption rate, estimated from TRAP-positive differentiated osteoclast numbers (Figure 2E), were increased, indicating high bone turnover. Histomorphometric analyses of $ER\alpha^{\Delta Oc/\Delta Oc}$ females supported the observation of accelerated bone resorption, as increased numbers of osteoclasts (Oc. S/BS and N. Oc/BS) were observed together with more eroded bone surface (ES/BS in Figure 2F). Bone formation was also enhanced as the rates of mineral apposition (MAR) and bone formation (BFR/BS) were both upregulated without an increase in osteoblast numbers (Ob.S/BS) (Figure 2F). Thus, considering all of these findings, it is conceivable that the increased number of differentiated osteoclasts following ERα ablation accelerates bone resorption over formation, leading to bone loss in the trabecular areas.

No Further Bone Loss Results from Estrogen Deficiency in $ER\alpha^{\Delta Oc/\Delta Oc}$ Females

To verify whether osteoclastic ERα indeed mediates osteoprotective estrogen actions, estrogen action was investigated by ovariectomy (OVX) of 12-week-old female mice. As expected, OVX in $ER\alpha^{+/+}$ females resulted in significantly reduced BMD particularly in the trabecular bone (Figures 3A and 3B) but not in the cortical bone (Figure 3C). Consistent with previous reports, (Kimble et al., 1995; Teitelbaum and Ross, 2003), estrogen deficiency following OVX upregulated the serum levels of cytokines like TNFα and IL-1α (Figure 3D). These cytokines enhance bone resorption through stimulation of osteoclastogenesis, leading to the loss of bone mass (Teitelbaum and Ross, 2003). OVX did not further reduce BMD or trabecular bone volume of the femurs of $ER\alpha^{\Delta Oc/\Delta Oc}$ females (Figure 3B) nor affect increased number of TRAP-positive osteoclasts (see lower panel in Figure 3A) despite upregulation of serum cytokines. This suggests that the expression of cytokines known to regulate bone resorption is not under the control of osteoclastic ERα.

Estrogen Treatment Failed to Rescue the Osteoporotic Bone Phenotype of $ER\alpha^{\Delta Oc/\Delta Oc}$ Mice

Estrogen treatment by estrogen pellet implantation (OVX + E2) for 2 weeks after OVX in $ER\alpha^{+/+}$ mice elicited a dramatic increase in bone mass in both the trabecular and cortical areas of the femurs (data not shown) and lumbar vertebral bodies (Figure 4A). Estrogen action during E2 treatment in female mutants ($ER\alpha^{\Delta Oc/\Delta Oc}$) was not as pronounced as in the $ER\alpha^{+/+}$ females (Figures 4A and 4B), and the increase in the trabecular portions of the distal femurs was slight (data not shown). Histomorphometric analysis of the lumbar vertebral bodies (Figure 4B) supported the idea that E2 treatment in the female mutants was not sufficient to suppress accelerated bone resorption. These in vivo findings in the $ER\alpha^{\Delta Oc/\Delta Oc}$ females suggest that in at least the trabecular areas of the long bones and lumbar vertebral bodies, the osteoprotective estrogen action is primarily mediated via osteoclastic ERα inhibiting bone resorption.

To further test this hypothesis, we investigated ERα protein expression in mature osteoclasts from trabecular bone. Few reports document osteoclastic expression of ERα protein and an estrogen response in both intact animals and in in vitro cultured osteoclasts (Bland, 2000). We therefore reasoned that ER expression ceases during differentiation into mature cells from primary cultures of osteoclast precursors, similar to that observed in other primary culture cell systems such as avian oviduct cells, in which ERα protein expression is drastically decreased during culture (Kato et al., 1989). Using highly sensitive immunohistochemistry, we investigated whether

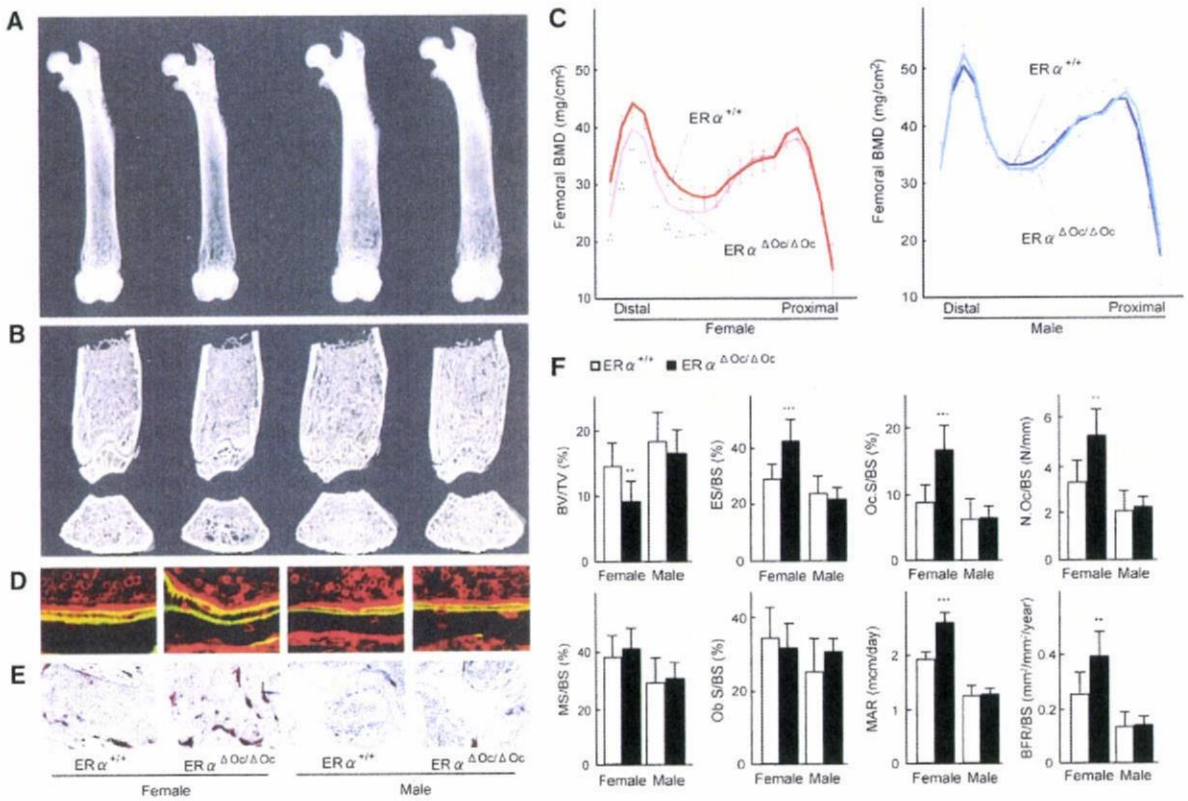

Figure 2. High Bone Turnover Osteopenia Was Observed in $ER\alpha^{\Delta Oc/\Delta Oc}$ Females But Not Males

(A) Soft X-ray images of femurs from 12-week-old $Ctsk^{Cre/+}$; $ER\alpha^{flox/flox}$ ($ER\alpha^{\Delta Oc/\Delta Oc}$) mice.

(B) Three-dimensional computed tomography images of the distal femurs and axial sections of distal metaphysis from representative 12-week-old $Ctsk^{Cre/+}$; $ER\alpha^{+/+}$ ($ER\alpha^{+/+}$) and $ER\alpha^{\Delta Oc/\Delta Oc}$ mice.

(C) BMD of each of 20 equal longitudinal divisions of femurs from 12-week-old $ER\alpha^{+/+}$ and $ER\alpha^{\Delta Oc/\Delta Oc}$ mice. (n = 10–11 animals per genotype; Student's t test, *p < 0.05; **p < 0.01; ***p < 0.001). Data are represented as mean ± SEM.

(D) Bone formation was also accelerated in $ER\alpha^{\Delta Oc/\Delta Oc}$ females when two calcein-labeled mineralized fronts visualized by fluorescent micrography were measured in the proximal tibia of 12-week-old mice.

(E) The number of TRAP-positive osteoclasts in the lumbar spine of female mice was increased by selective disruption of ERα in osteoclasts, indicating enhanced bone resorption.

(F) Bone turnover parameters as measured by dynamic bone histomorphometry after calcein labeling indicated high bone turnover in $ER\alpha^{\Delta Oc/\Delta Oc}$ females. Parameters are measured in the proximal tibia of 12-week-old $ER\alpha^{+/+}$ (open column) and $ER\alpha^{\Delta Oc/\Delta Oc}$ (filled column) mice. BV/TV: bone volume per tissue volume. ES/BS: eroded surface per bone surface. Oc.S/BS: osteoclast surface per bone surface. N.Oc/BS: osteoclast number per bone surface. MS/BS: mineralizing surface per bone surface. Ob.S/BS: osteoblast surface per bone surface. MAR: mineral apposition rate. BFR/BS: bone formation rate per bone surface (n = 10–11 animals per genotype; Student's t test, *p < 0.05; **p < 0.01; ***p < 0.001). Data are represented as mean ± SEM.

ERα protein expresses in differentiated osteoclasts in the bone tissues of femur sections from 12-week-old mice. ERα protein expression appeared abundant in osteoblasts and osteocytes of femur sections (Figure 4C) as well as hypothalamus (Figure S2B) from 12-week-old mice, in agreement with a previous report (Zaman et al., 2006). Likewise, expression levels of ERα in primary cultured osteoblasts derived from calvaria of $ER\alpha^{\Delta Oc/\Delta Oc}$ females appeared unaffected (Figure S2C). In contrast, in differentiated osteoclasts of the same femur sections, ERα expression was definitely detectable but very low in the $ER\alpha^{+/+}$ but undetectable in $ER\alpha^{\Delta Oc/\Delta Oc}$ females (Figure 4C).

Signaling by Osteoclastogenic Factors and Osteoclastogenesis Is Intact in Osteoclasts Deficient in ERα

It is possible that the osteoprotective function of osteoclastic ERα inhibits osteoclastogenesis. To address this issue, osteoclastogenesis was tested in cultured osteoclasts derived from bone-marrow cells of $ER\alpha^{\Delta Oc/\Delta Oc}$ mutants. In this cell culture system, a possible contribution of contaminated immune cells and stromal cells could be excluded, since osteoclastogenesis is only inducible by M-CSF treatment followed by M-CSF + RANKL (Koga et al., 2004).

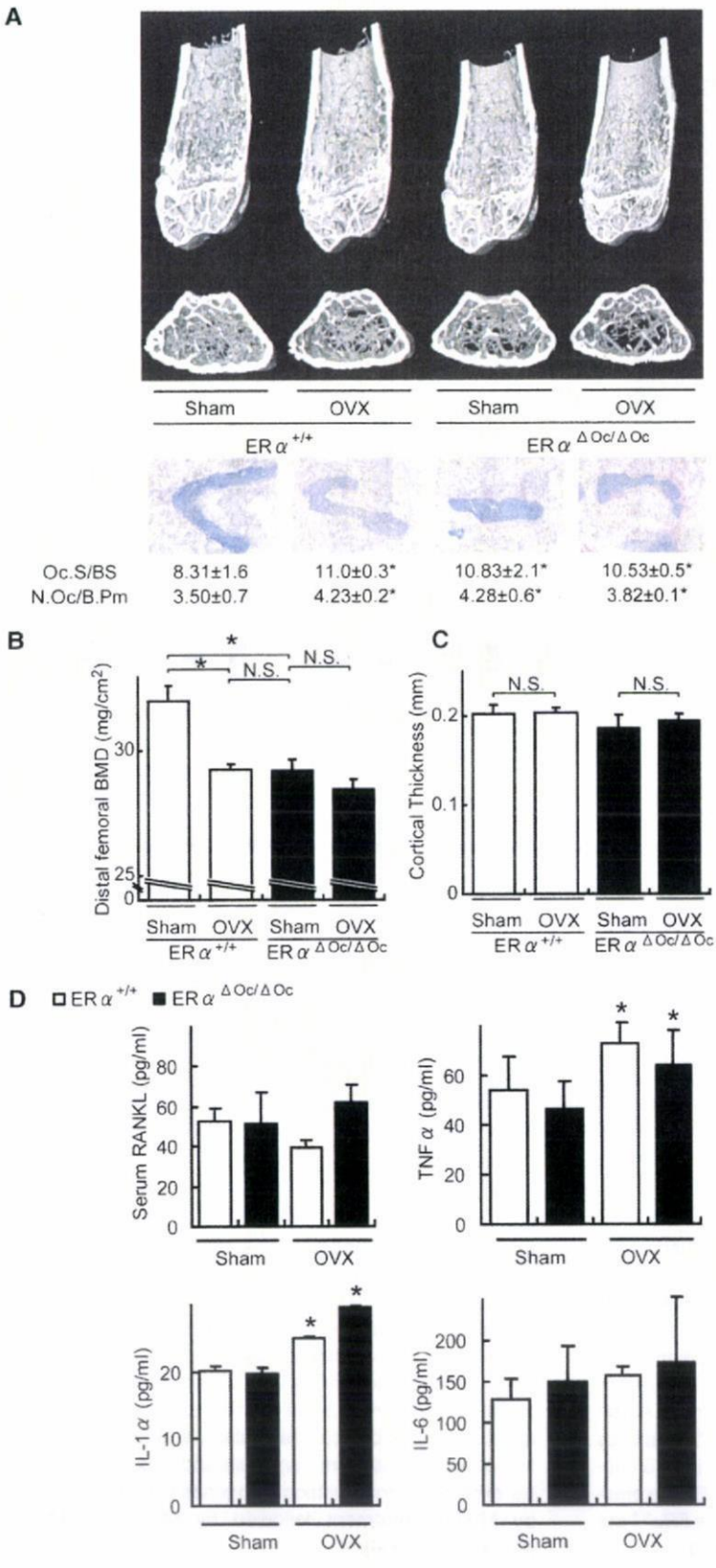

Figure 3. No Further Bone Loss of $ER\alpha^{\Delta Oc/\Delta Oc}$ Females by Ovariectomy

(A) Distal femoral micro CT analysis and lumbar vertebral bone histomorphometrical analysis of sham-operated or ovariectomized (OVX) 12-week-old $ER\alpha^{+/+}$ and $ER\alpha^{\Delta Oc/\Delta Oc}$ mice (*$p < 0.05$ compared to $ER\alpha^{+/+}$ sham group). Two weeks after OVX, the bone phenotype was analyzed.

(B) BMD of the distal femurs within each group are described in Figure 3A (*$p < 0.05$; N.S., not significant). Data are represented as mean ± SEM.

(C) Cortical thickness evaluation from micro CT analysis of femurs within each group described in Figure 3A. Data are represented as mean ± SEM.

(D) The levels of TNFα, IL-1α, and IL-6 in the bone-marrow cells culture media and serum RANKL (*$p < 0.05$ compared to each sham group). Data are represented as mean ± SEM.

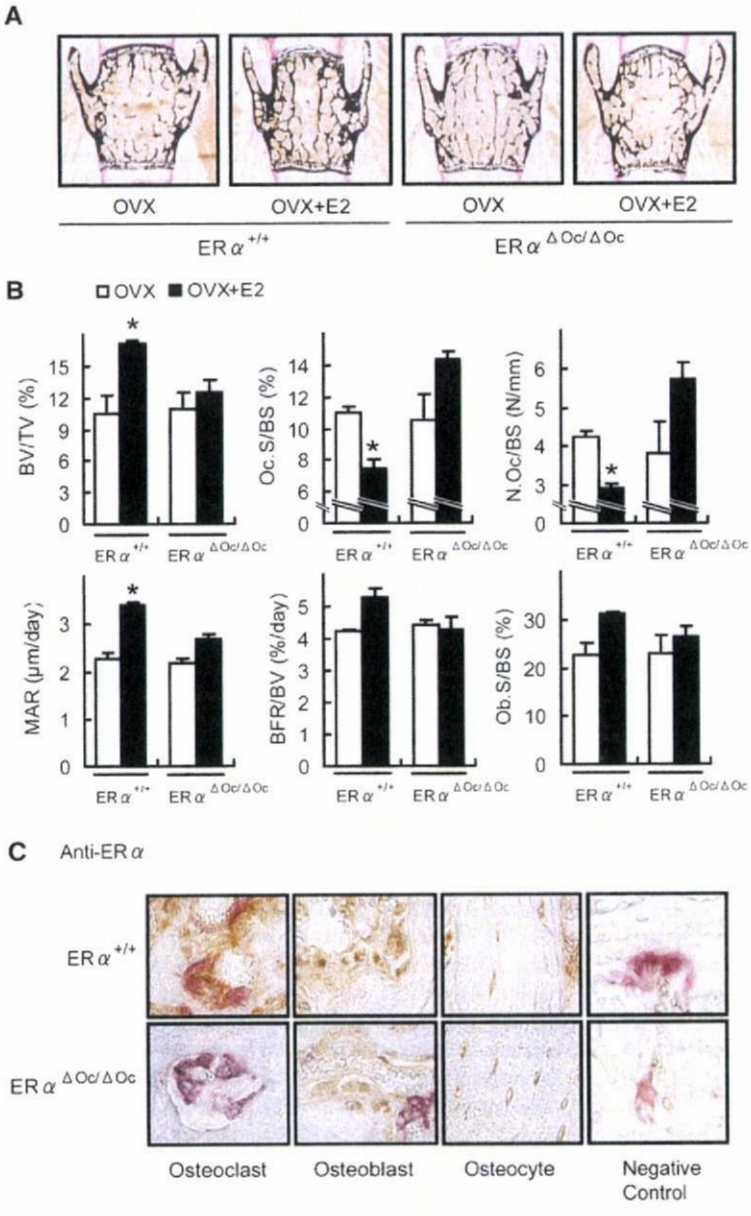

Figure 4. Estrogen treatment failed to reverse trabecular bone loss of ovariectomized $ER\alpha^{\Delta Oc/\Delta Oc}$ females

(A) von kossa staining of lumbar vertebral bodies of ovariectomized $ER\alpha^{+/+}$ and $ER\alpha^{\Delta Oc/\Delta Oc}$ mice treated with or without 17β-estradiol (0.83 μg/day) for 2 weeks (+E2) groups.

(B) Bone histomorphometrical analyses of the lumber vertebral bodies of 12-week-old ovariectomized $ER\alpha^{+/+}$ (left columns) and $ER\alpha^{\Delta Oc/\Delta Oc}$ (right columns) mice with (filled columns) or without (open columns) E2 treatment for 2 weeks (*$p < 0.05$ compared with E2-treated ovariectomized $ER\alpha^{\Delta Oc/\Delta Oc}$ mice). BV/TV: bone volume per tissue volume. ES/BS: eroded surface per bone surface. Oc.S/BS: osteoclast surface per bone surface. N.Oc/BS: osteoclast number per bone surface. MS/BS: mineralizing surface per bone surface. Ob.S/BS: osteoblast surface per bone surface. MAR: mineral apposition rate. BFR/BS: bone formation rate per bone surface. Data are represented as mean ± SEM.

(C) Immunochemical identification of ERα (brown) in TRAP-positive (red) differentiated osteoclasts. The femurs of 12 week-old mice were used for the immunodetection of ERα in bone cells. All labels were abolished when the primary antibody was preadsorbed with the immunizing peptide (negative control).

The number of TRAP-positive osteoclasts differentiated from the bone-marrow cells of $ER\alpha^{\Delta Oc/\Delta Oc}$ females was almost the same as that from $ER\alpha^{+/+}$ females (Figure 5A) and males (data not shown). The differentiated $ER\alpha^{\Delta Oc/\Delta Oc}$ osteoclasts had typical osteoclastic features, including the characteristic cell shape, TRAP-positive, multiple nuclei, and actin-ring formation, and were indistinguishable from the $ER\alpha^{+/+}$ osteoclasts (Figure 5B).

The expression levels of the prime osteoclastogenic transcription factors, c-*fos* and *NFATc1*, were unaltered by ERα deficiency in differentiated osteoclasts (Figure 5C). Furthermore, responses to RANKL in intracellular signaling, as represented by phosphorylation of p38 and IκB, were unaffected in $ER\alpha^{\Delta Oc/\Delta Oc}$ osteoclasts from females (Figure 5D) as well as males (data not shown). In light of these findings, it is unlikely that activated ERα in osteoclastic cells attenuates osteoclastogenesis.

Activation of the Fas/FasL System by Estrogen in Intact Bone Is Impaired by Osteoclastic ERα Deficiency

To examine osteoclastic ERα function in intact bone, DNA microarray analysis following real-time RT-PCR of RNA from the femurs of ovariectomized $ER\alpha^{\Delta Oc/\Delta Oc}$ females treated with or without estrogen, was performed. During

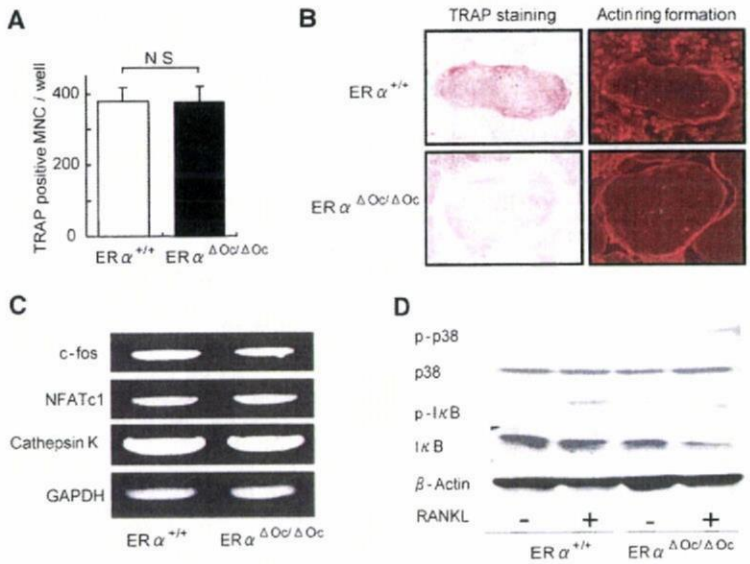

Figure 5. ERα Deficiency Did Not Affect Osteoclastogenesis

(A) TRAP-positive multinucleated cell count at 3 days after RANKL stimulation, cultured in 24-well plates (n = 6, N.S., not significant). Data are represented as mean ± SEM.

(B) TRAP staining and actin ring formation of RANKL induced primary cultured osteoclasts from bone-marrow cells of $ERα^{+/+}$ and $ERα^{ΔOc/ΔOc}$ mice.

(C) RT-PCR analysis of genes related to osteoclastogenesis.

(D) Western blot analysis of phosphorylated p38, JNK, and IκB of primary cultured bone-marrow cells stimulated with or without 100 ng/ml of RANKL for 15 min.

the search for candidate ERα target genes in bone by DNA microarray analysis (Figure S3), we found that a number of apoptosis-related factors were regulated by estrogen in the intact bone of $ERα^{+/+}$ females but dysregulated in $ERα^{ΔOc/ΔOc}$ females. This observation is consistent with a previous report of estrogen-induced apoptosis of mature osteoclasts (Kameda et al., 1997). Real-time RT-PCR to validate the estrogen regulations of the candidate genes revealed that gene expression of *FasL*, an apoptotic factor, was responsive to E2 (Figure 6A). Estrogen treatment (+E2) indeed induced expression of FasL protein in bone of ovariectomized $ERα^{+/+}$, but this induction was not obvious in ovariectomized $ERα^{ΔOc/ΔOc}$ mice (Figures 6B and 6C). Reflecting FasL induction by estrogen, estrogen-induced apoptosis (as observed by the TUNEL assay) in TRAP-positive mature trabecular osteoclasts in the distal femurs of the $ERα^{+/+}$ mice was detected, but this E2 response was abolished in the $ERα^{ΔOc/ΔOc}$ mice (Figure 6D). Furthermore, in mice lacking functional FasL ($FasL^{gld/gld}$), neither enhanced bone resorption nor bone mass loss was induced by ovariectomy (Figures 6E and 6F).

Osteoclastic ERα Mediates Estrogen-Induced apoptosis by FasL

The expression level of ERα protein in differentiated osteoclasts derived from bone marrow cells was very low, but induction of *FasL* gene expression was also detectable in the cultured osteoclasts of $ERα^{+/+}$ females as well as males (Figure 7A). However, this E2 response was impaired in cultured osteoclasts from $ERα^{ΔOc/ΔOc}$ females (Figure 7A). It is notable that such responses are also induced by tamoxifen (Figure 7C), which is an osteoprotective SERM (Harada and Rodan, 2003). ERα overexpression augmented *FasL* gene expression in response to estrogen in cultured osteoclasts from $ERα^{ΔOc/ΔOc}$ females (Figure S4A). In primary cultured calvarial osteoblasts from females as well as males (Suzawa et al., 2003), *FasL* gene induction by E2 and tamoxifen was also seen; however, it was not accompanied by increased apoptosis (data not shown). Thus, it appears that estrogen-induced apoptosis in osteoclasts is mediated by FasL expression in osteoclasts in the trabecular bone areas, presumably as well as in osteoblasts in cortical bone areas. As expected, the cell number of TUNEL-positive osteoclasts was increased by E2 in the cultured osteoclasts from $ERα^{+/+}$ females, but E2-induced apoptosis was undetectable in $ERα^{ΔOc/ΔOc}$ osteoclasts (Figure 7B). Consistent with FasL-induced apoptosis, *Fas* gene expression was observed (Figure 7D), but it was likely that Fas expression did not require ERα function (Figures S4B and S4C). Expression levels of *Fas* and *ERα* as well as E2 response in apoptosis appeared to fluctuate during osteoclast differentiation (Figures S4B–S4D); however, in FasL mutant ($FasL^{gld/gld}$) females, the E2-induced apoptosis was abolished (Figure S4E). These findings suggest that activated ERα in differentiated osteoclasts induces apoptosis through activating FasL/Fas signaling. This leads to suppression of bone resorption through truncating the already short life span of differentiated osteoclasts (Teitelbaum, 2006).

DISCUSSION

Selective ablation of ERα in mature osteoclasts in female mice shows that the osteoprotective effect of estrogen is mediated by osteoclastic ERα, at least in the trabecular regions of the tibiae, femur, and lumbar vertebrae of female mice. Activated ERα by estrogen as well as SERMs appears to truncate the already short life span (estimated at 2 weeks) of differentiated osteoclasts by inducing apoptosis through activation of the Fas/FasL system.

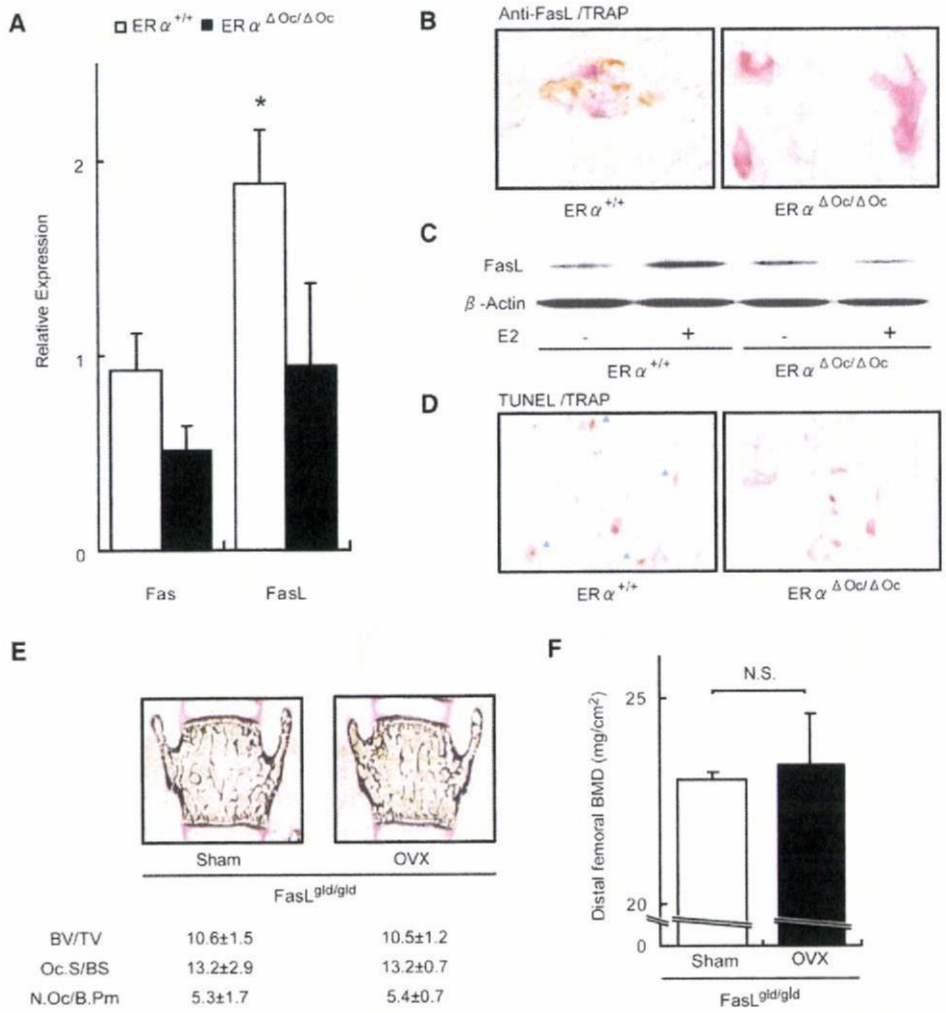

Figure 6. Activated ERα Induced Fas Ligand Expression and Apoptosis in Differentiated Osteoclasts of Intact Bone

(A) Real-time RT-PCR analysis of *Fas* and *FasL*. Expression levels in bones from E2-treated ovariectomized $ER\alpha^{+/+}$ (open column) and $ER\alpha^{\Delta Oc/\Delta Oc}$ (filled column) were compared with the ovariectomized groups of each genotype without E2 administration (*$p < 0.05$ compared to $ER\alpha^{+/+}$). Data are represented as mean ± SEM.

(B) Immunohistochemical analysis of anti-FasL with TRAP staining of the sections from the distal femurs of E2-treated ovariectomized $ER\alpha^{+/+}$ and $ER\alpha^{\Delta Oc/\Delta Oc}$ mice. Brawny stained cells are anti-FasL positive.

(C) Anti-FasL western blot analysis of proteins obtained from femurs of ovariectomized $ER\alpha^{+/+}$ and $ER\alpha^{\Delta Oc/\Delta Oc}$ mice treated with or without E2, using anti-β-actin as internal control.

(D) TUNEL staining with TRAP staining of the sections from the distal femurs of E2-treated ovariectomized $ER\alpha^{+/+}$ and $ER\alpha^{\Delta Oc/\Delta Oc}$ mice. Arrowheads indicate both TUNEL (brown)- and TRAP-positive staining cells.

(E) Bone histomorphometrical analysis of sham-operated or ovariectomized $FasL^{gld/gld}$ mice.

(F) BMD of the distal femurs of sham operated or ovariectomized $FasL^{gld/gld}$ mice. Data are represented as mean ± SEM.

This attenuates bone resorption. This idea is supported by previous observations that estrogen deficiency following menopause or ovariectomy leads to high bone turnover, particularly in the trabecular areas, as bone is rapidly lost through enhanced resorption (Delmas, 2002; Tolar et al., 2004). Thus, estrogen treatment leads to recovery from osteopenia by reducing resorption (Delmas, 2002; Rodan and Martin, 2000), partly by the induction of osteoclast cell death.

In contrast to the osteopenia seen in the $ER\alpha^{\Delta Oc/\Delta Oc}$ females, the $ER\alpha^{\Delta Oc/\Delta Oc}$ male mice unexpectedly had no bone loss. The male mice still demonstrated an ERα-mediated induction of FasL in response to estrogen with subsequent apoptosis of osteoclasts (Figure 7). Both male mice with a deficiency of aromatase that are unable to locally produce estrogen from testosterone and men with a genetic mutation in the *ERα* gene suffer from osteoporosis (Smith et al., 1994). Considering that the